Technische Universität München
Lehrstuhl für Elektrische
Energiespeichertechnik
Prof. Dr.-Ing. Andreas Jossen

Performance Analysis of Lithium-Ion Cells in Different Packaging Geometries

Master thesis

of

Ayush Sengupta

Supervisor:
M.Sc. Yao Wu

DD. MMMM YYYY

Abstract

Lithium-ion cells with a $LiFePO_4$ cathode and a graphite anode are gaining popularity among lithium battery technologies because of enhanced safety and low cost. But they still suffer from disadvantages like reduced energy and power density. Although a lot of research is going on to improve these cells, the research on the impact of packaging geometries on the cell performance is still minimal. While cylindrical and prismatic cells are the most popular, pouch cells are less used in industrial applications despite the advantages of higher energy density and flexibility. Commercially, cells of the three geometries have different materials and different rated capacities which makes an accurate comparison much difficult. This thesis aims to analyze the performance and effect of different packaging geometries of cells manufactured specifically with the same materials and the same rated capacities.

The thesis is restricted to cyclic aging tests. First, the performance of unaged cells conditioned at 0.3C, 5°C was analyzed with respect to direct current (DC) pulse tests for segregating the internal resistances and polarizations, and temperature developed over the cycles. It was observed that pouch cells showed the least internal resistances while prismatic cells showed the highest. Pouch cells showed a very steep rise in internal resistances at the end of the discharge cycle. The temperature rise was relatively low due to a low maximum C-rate of 2C for cycling (maximum 10.40 K increase for prismatic cells). As expected from the trend of ohmic resistances, prismatic cells reached highest temperatures with pouch cells showing the lowest high temperatures. DC pulse tests of aged cells showed that a rapid increase in internal resistance in the case of pouch cell was found to set in at a very later stage as compared to the other two geometries. Further, for cylindrical and prismatic cells, diffusion related phenomena are affected the most by aging. The study of aging mechanisms showed evidence of early-stage lithium plating for cylindrical and prismatic cells at low temperatures of cycling, and the possibility of loss of active material (LAM) at later stages due to electrode deterioration. Pouch cells showed the best capacity retention and evidence to prove the most stable and uniform solid-electrolyte interface (SEI) layer formation. The optimum temperature of cycling was found to be highest for cylindrical cells and least for pouch cells. In the end, the thesis also discusses strategies for a more thorough comparison of the geometries. The main purpose of the work is to pave way for further research in this area and extend it to practical applications.

Index

Abbreviation register

DOD ..... Depth of Discharge
DVA ..... Differential Voltage Analysis
ECU ..... Extended Check-Up
EFC ..... Equivalent Full Cycles
EOL ..... End of Life
ESS ..... Energy Storage Systems
EV ..... Electric Vehicles
IRR ..... Internal Resistance Ratio
LFP ..... $LiFePO_4$
LTO ..... Lithium titanium oxide
NiCd ..... Nickel-Cadmium
NiMH ..... Nickel-metal hydride
OCV ..... Open Circuit Voltage
SCU ..... Short Check-Up
SEI ..... Solid Electrolyte Interface
SOC ..... State of Charge
SOH ..... State of Health

1 Introduction

Global rise in consumer electronics, automation and smart technologies has necessitated the use of battery energy storage systems. Among all, lithium-ion battery technologies have found applications from small consumer electronics to large stationary storage systems. They are widely used especially in electric vehicles (EVs) with humans moving towards a greener future. But the lithium-ion batteries used in EVs are very expensive. This necessitates the need for further research on reducing costs and achieving optimal functionality. Another important aspect to be taken care of is the safety issue. Many of the early lithium-ion technologies are prone to thermal runaway which not only damages the battery itself but also can be hazardous. The collaborative research project, SPICY aims at the development of new generation of lithium-ion batteries that have improved performance and safety at low costs. It particularly involves performance improvement of lithium-ion cells with $LiFePO_4$ (LFP) cathode. $LiFePO_4$ is found to be safer and more durable than other cathode materials like $LiCoO_2$ but $LiFePO_4$ has a lower energy density.

The LFP-graphite cells are available in different packaging geometries: cylindrical, prismatic and pouch. These geometries offer different properties like the difference in weight, energy density, and packaging efficiencies. Different EV manufacturers use different packaging geometries for their vehicles. Nissan Leaf and BMW i3 are known to use the prismatic cells [1]. The electric vehicle pioneer, Tesla Motors, uses cells with a cylindrical packaging (traditionally, the 18650-type and more recently, the 21700-type) [2]. Production vehicles, such as Daimler Smart, Renault Zoe and Nissan Leaf, use cells with pouch type packaging geometry [2].

While each design has clear advantages and disadvantages, there is no winner on overall performance for mass-market EVs [3]. Cylindrical cells are still the most matured technology compared to the others. While the use of prismatic cells is also on the rise for different battery technologies, pouch cells were introduced for its reduced weight. Research has been done for many different commercial cells with respect to their performance, safety and reliability. The temperature developed in the cells or the capacity deterioration mechanisms have been widely studied. The research also includes study of different commercial cells of different geometries. But this does not provide a fair comparison of the performance of the cells in

different geometries. This is because the commercial cells researched and compared are either of different materials or have different capacities. Dedicated research based on performance and aging of cells is lacking in which the cells have different packaging geometries but the same material and deliver the same capacities. Therefore, the core purpose of the thesis is to analyze cells which are based on the LFP-graphite electrodes and a rated capacity of 16 Ah but differ only in their packaging geometries. Thus, the results of the study should logically compare the packaging geometries. As a long-term scope, the results can help further research which may eventually determine the suitability of geometries for specific applications.

During the thesis, the data was obtained from various tests performed by different partner organizations of the SPICY project, as mentioned earlier. State-of-the-art methods were used for the cell manufacture. Care was taken to maintain uniformity with respect to chemistry and capacity sizing of the various geometries for a fair comparison. The data obtained was then sorted, analyzed and visualized using MATLAB. Several assumptions were made across the cell analysis for ease of comparison and data visualization. Further, the experimental results were attempted to be validated and inferences were made based on past research by peers.

The thesis is arranged into different chapters. First, the fundamentals of lithium-ion technology are discussed especially with respect to LFP-graphite based cells and a discussion on the different geometries of packaging and the existing knowledge about their comparison. The next chapter discusses literature reviewed on performance analysis of the geometries of the cell. It also includes a discussion of the literature on the performance and aging mechanism of lithium-ion cells, especially those relevant to the thesis work. In the subsequent chapter, the different cells used during the experiments are described followed by detailing the setup of the experiments. This is followed by a discussion of the experiment results and inference based on the literature reviewed before. The core part of the thesis ends with conclusions drawn from the results, a discussion of limitations of the work and the scope for future research and improvements.

2 Lithium-ion Batteries and Packaging Geometries

This chapter briefly introduces the lithium-ion battery technology in general, followed by a discussion of the LFP-graphite based cells and an introduction to the packaging geometries. This chapter serves as the knowledge foundation for the rest of the work.

2.1 Lithium-ion technology

Lithium-ion batteries play a significant role in present-day energy storage systems, primarily due to their high energy density and high specific energy. Invented by the American physicist Professor John Goodenough in 1980 as a new type of battery in which the lithium could transport through the battery from one electrode to the other as a Li^+ ion, it was first commercially introduced as a product by Sony Corporation [4] [5]. The simple basis of these batteries is that a compound of lithium with a transition metal - such as nickel, manganese, cobalt, iron - and oxygen forms the cathode, whereas, graphite or lithium-titanium oxide (LTO) is the anode [4].

The chemical properties of lithium make it advantageous over other technologies. Due to its lowest reduction potential of all elements, lithium-ion cells have the highest available cell potential. Lithium being one of the lightest element and having one of the smallest radii, lithium-based batteries have high gravimetric and volumetric capacity and power density [6]. Therefore, despite disadvantages like high costs and possible high-temperature development, the above advantages make it very desirable for many commercial and research-related activities. This prompts for further studies and experiments to improve safety and reducing the costs of lithium-ion batteries.

Lithium-ion batteries contain lithium-based cathodes and graphite-based anodes, making them lighter than other types of rechargeable batteries. Lithium is highly reactive and has the potential to store high energies. Lithium-ion batteries retain their capacities for longer periods of time, that is, they have low self-discharge. Lithium-ion batteries do not have to be completely discharged before recharging to retain full charge capacity, which is the case in some batteries like NiCd (Nickel-Cadmium). Lithium-ion batteries have long cycle lives and can retain a large number of charge-discharge cycles without large losses in capacity [7].

However, lithium-ion cells have a few disadvantages as well. The service life or shelf life of a lithium-ion battery decreases with aging even when it is not in use. This means that from the time of manufacturing, regardless of the number it was cycled, the capacity of a lithium-ion battery will decline gradually. An increase in internal resistance is also observed with aging these cells. They are more sensitive to high temperatures than most other chemistries like NiMH (Nickel-metal hydride) or NiCd. While NiCd has extreme temperature tolerance, NiMH works well in medium-to-high temperatures [8]. Hot storage and operating conditions cause lithium-ion battery packs to degrade much faster than they normally would. Lithium-ion batteries can be severely damaged by deep discharge, i.e., by discharging them below the minimum voltage threshold recommended by the manufacturer. Consequently, lithium-ion battery packs come with an onboard circuit to manage the battery. This makes them even more expensive than they already are. In general, lithium-ion chemistry is not as safe as NiCd or NiMH. This is because the anode produces heat during use, while the cathode produces oxygen (though not for all lithium-ion chemistries). The safety problem in lithium-ion batteries has been attributed to thermal runaway. It is initiated by a powerful exothermic reaction of recombination of atomic hydrogen accumulated in anode graphite during the cell cycling. NiMH, on the other hand, have much less active materials than lithium-ion cells [7] [9]. Table 2.1 shows a comparison of lithium-ion batteries with other technologies.

Table 2.1. Comparison of different battery technologies [10]

Cathode	**Lithium-ion**	**Pb-acid**	**Ni-Cd**	**Ni-MH**
Cycle life	500-1000	200-500	500	500
Working potential (V)	3.6	1.0	1.2	1.2
Specific energy (Wh/kg)	100	30	60	70
Specific energy (Wh/L)	240	100	155	190

Currently, lithium-ion technologies are used in a variety of applications, especially in portable electronics, EVs and power tools. The high energy efficiency of lithium-ion batteries makes them useful in electric grids, where they contribute to the quality of energy harvested from wind, solar, geo-thermal and other renewable sources. It promotes widespread use of renewable energy sources and building an energy-sustainable economy [6].

Because of lithium's ability to form compounds with a variety of transition metals and oxygen, different types of lithium-ion battery technologies are available. Table 2.2 shows some typical properties and applications of the most commonly used types of lithium-ion batteries:

Table 2.2. Typical properties and applications of different types of lithium-ion cells [11]

	Li-Cobalt (LCO)	**Li-Manganese (LMO)**	**Li-Nickel Manganese Cobalt (LNMC)**	**Li-Iron Phosphate (LFP)**
Specific energy (Wh/kg)	150-200	100-150	150-220	90-120
Nominal voltage (V)	3.6	3.7	3.7	3.3
Cycle life	500-1000	300-700	1000-2000	1000-2000
Application	Mobile phones, tablets, laptops, cameras	Power tools, medical devices, electric powertrains	E-bikes, medical devices, EVs, industrial	Portable and stationary needing high load currents and endurance

The advantages of lithium-ion cells far outweigh the disadvantages in terms of commercial usage which necessitates the need for research to understand and alleviate the shortcomings of the technology. Such research work led to the development of $LiFePO_4$|C (LFP-GRAPHITE) cells which is known to be low cost and offers safety, stability and reliable performance. LFP-GRAPHITE or LFP-graphite cells form the basis of studies in this thesis. The next sub-section introduces and discusses a typical LFP-graphite cell, its geometry, and chemistry in general.

2.2 $LiFePO_4$-graphite cells

John B. Goodenough research group at the University of Texas first published literature in 1996 about the use of $LiFePO_4$ as an electrode for lithium-ion cells [12]. Despite disadvantages like low electrical conductivity and slow lithium-ion diffusion, LFP-graphite is one of the safest and cheapest lithium-ion technologies. LFP-graphite cells have found

application in EVs, stationary storage systems and power backup systems [13]. It consists of a LFP cathode along with a graphitic carbon anode. $LiFePO_4$ based cathodes, while having less energy density, have better longevity as compared to other cathode materials like $LiCoO_2$ [14]. To further discuss the chemistry of LFP-graphite cells, Figure 2.1 introduces a schematic of the ion-transport in the cell.

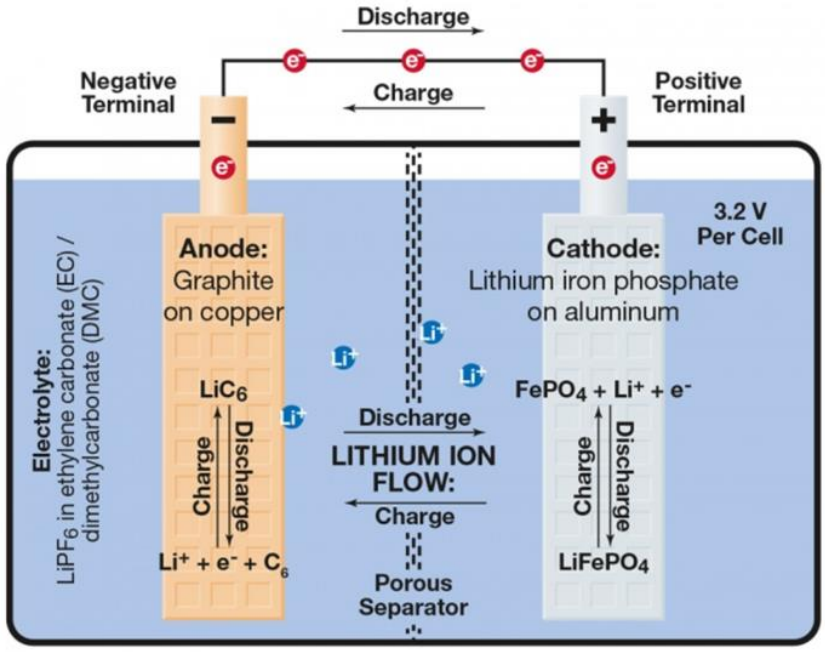

Figure 2.1. Schematic diagram of ion-transport in a LFP-graphite cell [14]

Each cell consists of an anode of graphite on copper current collectors and a cathode of $LiFePO_4$ on the aluminum collectors. Between them there is electrolyte containing dissociated lithium salts (for example, $LiPF_6$ in ethylene carbonate/dimethyl carbonate), which enables transport of lithium ions between the two electrodes [14] [15]. The separator isolates the two electrodes and is a membrane that allows transport of ions from the cathode to the anode during charge (reverse during discharge).

It must be noted that lithium batteries are different from lithium-ion batteries. While lithium-ion batteries use a lithium compound as the cathode, lithium batteries use pure lithium metal as the cathode. Lithium batteries have much larger capacities and energy densities as compared to lithium-ion cells. But, since lithium is a highly reactive element, using pure lithium metal as an electrode makes it less safe as compared to lithium-ion. Further, lithium batteries are not rechargeable. These two disadvantages are why lithium-ion cells were developed and are the focus of the study done here.

Equation (2.1) represents the general chemical reaction in a LFP-graphite cell. While the forward process shows the deintercalation of lithium-ions to charge the cathode, the reverse process shows the discharge process [10].

$$LiFePO_4 - x\,Li^+ - x\,e^- \leftrightharpoons x\,FePO_4 + (1-x)\,LiFePO_4 \tag{2.1}$$

The chemical reaction has been broken down to part reactions in Figure 2.2:

<table>
<tr><td colspan="2">$LiFePO_4 \leftrightharpoons FePO_4 + Li^+ + e^-$</td><td colspan="2">$Li^+ + e^- + 6C \leftrightharpoons LiC_6$</td></tr>
<tr><td>Cathode
($LiFePO_4$ on Al terminal)</td><td colspan="2">Electrolyte
$LiPF_6$ in ethylene carbonate (EC)/ dimethyl carbonate (DMC)</td><td>Anode
(Graphite on Cu terminal)</td></tr>
<tr><td colspan="2">Left to right → Charging</td><td colspan="2">Right to left ← Discharging</td></tr>
</table>

Figure 2.2. Part reactions involved in the chemistry of an LFP-GRAPHITE cell [14]

Figure 2.2 helps to understand the reactions taking place at each of the electrodes during charging and discharging, which is essential to explain the ion-electron movement across the cell and related electrochemical processes and resistances involved.

Jow et al. [16] [17] have discussed the Li^+ charge transfer process and the charge-discharge kinetics in detail. During charging, at the cathode side, an interaction between the cathode and the passivation layer formed on the cathode produces Li^+ and an electron. The electron travels across the electron conducting network within the electrode and reaches the electrode surface. The Li^+ is then transported to the negative electrode, in a solvated form (shown as "Li^+" in equation (2.3)). Next, at the negative electrode (anode), the de-solvation of this ion takes place whereby the "Li^+" sheds the solvated solvent molecules before transporting through the solid-electrolyte interface (SEI) on the anode surface. At the anode, the Li^+ takes an electron and intercalates into the anode surface. This whole process of charging is explained using the equations below [16]:

At the cathode,

- Li de-intercalation, dissolution from $LiFePO_4$ to become Li^+ and e^-

$$LiFePO_4 \rightarrow x\,Li^+ + x\,e^- + Li_{1-x}FePO_4 \tag{2.2}$$

- Li^+ transport through the passivation layer on cathode.
- Li^+ solvation in the electrolyte

$$Li^+ \rightarrow "Li^+" \tag{2.3}$$

At the anode,

- De-solvation of the "Li^+" at the SEI/electrolyte interface

$$"Li^+" \rightarrow Li^+ \tag{2.4}$$

- Li^+ transport through the SEI towards anode
- Li^+ reaching the anode and accepting an electron at the anode-SEI interface.

$$xLi^+ + xe^- + C_6 \rightarrow Li_xC_6 \tag{2.5}$$

During the discharge process, the steps are reversed. Jow et al. [17] also noted that the de-solvation process (equation (2.4) above) is the predominant limiting factor. Figure 2.3 illustrates the charge transfer during charging and discharging.

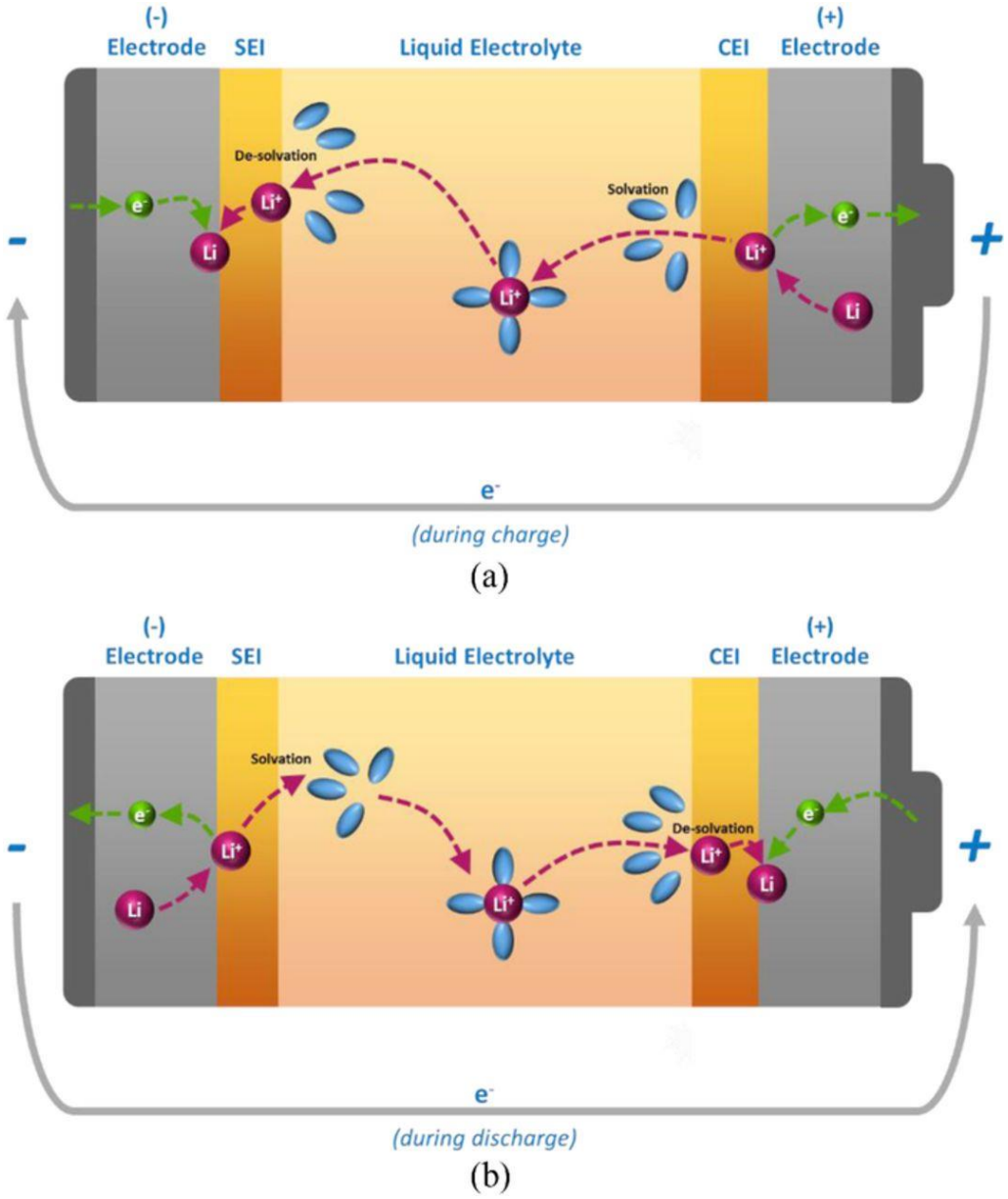

Figure 2.3. Charge transfer kinetics mechanism during (a) charge and (b) discharge [16]

In the initial stages of charging or discharging, the electrical or ohmic resistances dominate, while ionic or polarization resistances take over when the process continues. Polarization is the potential gradients developed as described in previous sections. These show up at different stages of a pulse test (as described earlier in this subsection), as they take different time durations to form. One such process is the formation of a concentration gradient in the presence of an electrolyte with a non-unity transport number, due to limitations in ion transport [18] [19]. The properties that determine how fast this gradient is formed are: diffusion coefficient, transport number, and thermodynamic enhancement number. The diffusion coefficient is usually determined based on electrolyte salt concentration gradients. The transport number is a measure of the fraction of the current being carried by the lithium-ion.

The thermodynamic enhancement factor is a measure of how the thermodynamic driving force relates to concentration gradients and depends on the activity coefficient [19]. It is understood that the mass transport concentration gradient is dependent on the chemical nature of the electrolyte.

Lithium-ion diffusion, on the other hand, in the active electrode material is directly related to the power density. The lithium-ion diffusion into and out of the electrode active material (intercalation and de-intercalation) is modeled using Fick's law of diffusion. $LiFePO_4$ have less lithium-ion diffusivity as compared to other cathode chemistries and therefore, is often doped with carbon. In addition to the chemical diffusion coefficient, the lithium diffusion depends on factors like porosity and tortuosity. Figure 2.4 below shows a typical porous electrode in lithium-ion cells. During charging, the Li^+ leaves the structure of $LiFePO_4$ and intercalates into the porous graphitic structure of the anode, while during discharge, it de-intercalates from the anode to remix with the cathode structure.

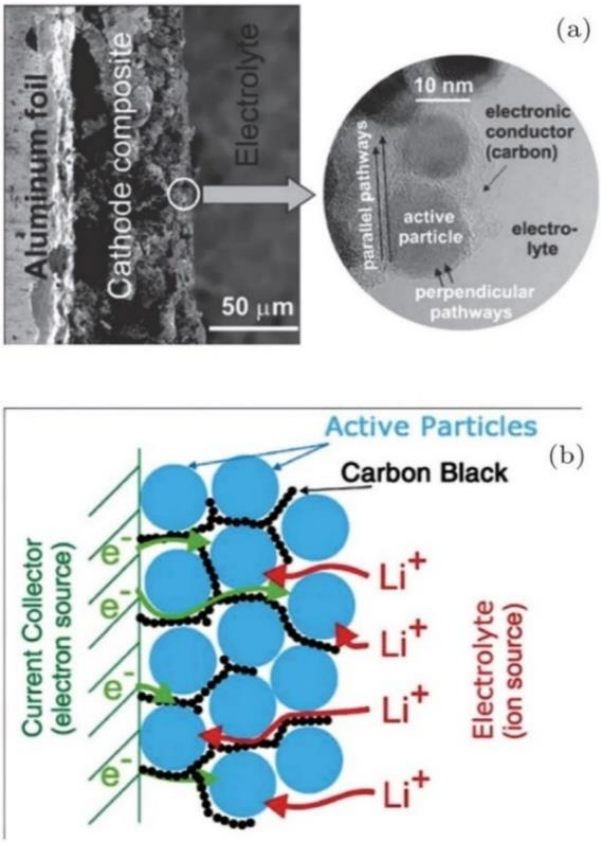

Figure 2.4. The porous electrode of a Lithium-ion battery (a) Low magnification (on left) and high magnification (inset on the right). (b) Schematics showing the main phases constituting a modern insertion cathode and its role in transport [20].

2.3 Packaging geometries of lithium-ion cells

The main aim of this thesis is to compare the different packaging geometries of lithium-ion cells. This subsection introduces and compares these geometries. Figure 2.5 shows components of the different geometries of lithium-ion cells.

Cylindrical geometry is the most common packaging technique for both primary and secondary cells. It has the main advantages of easy manufacturing and good mechanical stability. The tubular cylinder can withstand high internal pressures without deforming. But during battery arrangement, this geometry does not fully utilize the space by creating air cavities on side-by-side placement. Despite that, among all the commercial cells available today in the market, cylindrical cells are the most matured technology and provide the highest energy density. The higher energy density of the cylindrical cell compensates for its less ideal stacking abilities and the empty space can be used for cooling to improve thermal management. This cell design allows for added safety features that are not possible with other packaging designs. It cycles well, offers a long calendar life and is low in cost, but has comparatively low packaging density. It is available in several different sizes, with the 18650-type being the most popular. The nomenclature 18650 refers to an 18 mm diameter, a 65 mm height, while the last 0 refers to a cylindrical cell conforming to the IEC (International Electrotechnical Commission) standards. The other lithium-ion cylindrical formats commonly available commercially are 20700, 21700 and 22700 [21] [21].

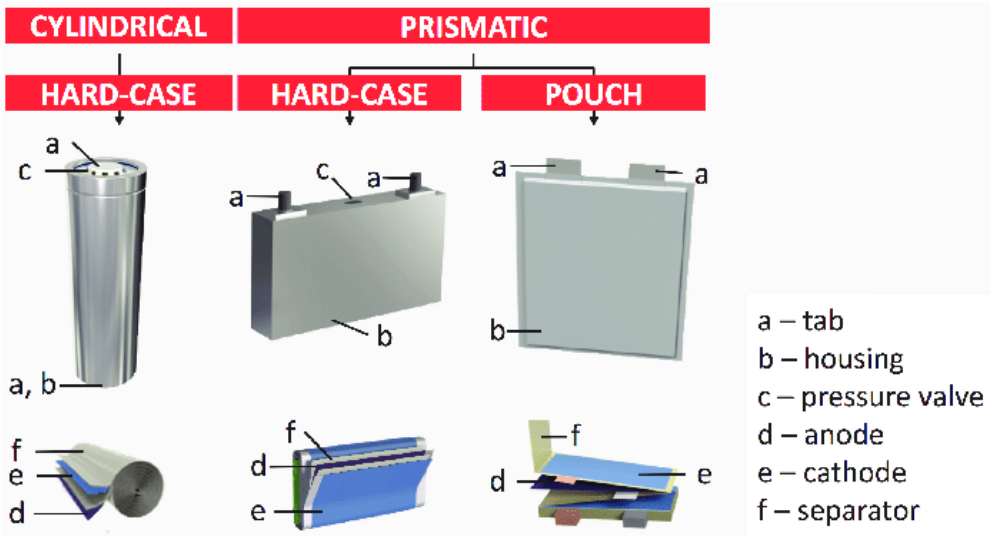

Figure 2.5. Diagram showing different geometries of lithium-ion batteries [22]

Prismatic cells are encased in aluminum or steel for stability. Jelly-rolled or stacked, the cell is space-efficient but can be costlier to manufacture than the cylindrical cell. The prismatic cell improves space utilization and allows flexible design. Whereas, according to the Polystor

Energy Corporation, it is found to be more expensive to manufacture, less efficient in thermal management, and have a shorter cycle life than the cylindrical design [21]. The manufacturing processes and construction of the three types of packaging geometries are explained in detail in Chapter 4.

The pouch cell offers a simple, flexible and lightweight solution to battery design. Some stack pressure is recommended but an allowance for swelling also must be made. The pouch cells can deliver high currents, but it performs best under light loading conditions and with moderate charging. It is cost-effective but exposure to humidity and high temperature can shorten life. Adding a light stack pressure prolongs longevity by preventing delamination. Swelling of 8–10 percent over 500 cycles must be considered with some cell designs [21]. It is estimated that in the future pouch cells will become cheapest to manufacture [21].

It has already been discussed that cylindrical cells are used in Tesla Motors electric vehicles, while prismatic cells are common in BMW i3 and pouch type geometry are used Daimler Smart and Renault Zoe. The following three figures show the arrangements of these geometries into battery packs in different EV cars.

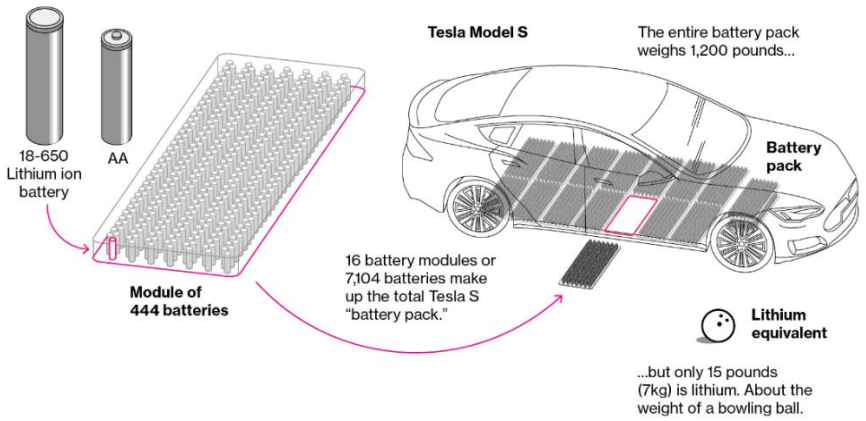

(a)

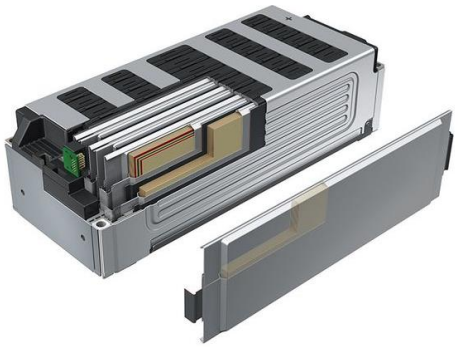

(b)

(c)

Figure 2.6. Battery pack arrangement for (a) Cylindrical [23], (b) Pouch [24], (c) Prismatic cells [24]

Figure 2.6 (a) shows 18650 cylindrical cell battery pack for the Tesla S model. Figure 2.6 (b) and Figure 2.6 (c) show the pouch and prismatic cell battery packs which are being developed by AUDI for their future electric cars. While the cylindrical cells leave behind some space from one cell to another due to their cylindrical shape, prismatic and pouch geometries show a more compact packaging, with the thin pouches providing scope for more flexibility.

Table 2.3. Comparison of cell packaging geometries [25]

Cylindrical	**Prismatic**	**Pouch**
+ Ease of manufacture + Good mechanical stability + Withstand high internal pressure + Lower cost (per W/h) + Long calendar life + Higher energy density	+ Thin profile (effective use of space) + Allows flexible design + Encased in metal/steel for stability	+ No need for metallic casing + Most efficient use of space + Lightweight
- Less space efficiency in battery packaging - Heavy	- Expensive to manufacture - Less efficient thermal management - Shorter cycle life - Deforms at high pressure - Higher cost (per W/h)	- Provision for swelling must be made - Cons like prismatic structure

While the use of these geometries in different EVs has already been discussed, they find different applications in other fields as well. Cylindrical cells mostly find use in portable applications and are used in power tools, medical instruments, laptops, and e-bikes. Prismatic cells are popular in cellphones, tablets and low-profile laptops electric powertrains, solar/wind storage uninterrupted power supply (UPS). Pouch cells are also used in portable applications like drones and hobby gadgets and in energy storage systems (ESS). Standardized pouch cells are not available and it gives the manufacturers the flexibility to design to their specific needs [25]. Each cell geometry has its own pros and cons in each application but currently, the scope itself is limited by the maturity of technologies with cylindrical cells being the most advanced and researched. Jaggi [25] summarizes the advantages and disadvantages of each type of cell geometry as shown in Table 2.3.

3 Literature Summary

Lithium-ion cells are taking over the storage market from low power to high power applications. The low reduction potential and low weight of lithium makes it suitable to be hosted by transition metals. These transition metals are Ti, V, Cr, Mn, Fe, Co, Ni and Cu [6]. That is why, lithium-ion cells can be built with many different cathode chemistries. The previous chapter discussed the benefits of using $LiFePO_4$ based cathodes. Many studies have been done to compare the different chemistries and different sizes of lithium-ion cells.

On the other hand, studies on the packaging geometries of the lithium-ion cells are limited. Pouch based packaging geometries, for example, are finding lots of applications in EVs. Pouch cells are even replacing cylindrical cells in many cases because of low weight and the improved energy density. Very few studies include a thorough comparison based on their performance analysis with respect to parameters like capacity evolution, internal resistance, differences in chemical changes during cycling. This chapter discusses the state of the art in research for the comparison study between the cell packaging geometries. The literature reviewed in this study is not just limited to LFP-graphite and lithium-ion cells but tries to incorporate relatable results from the work on other electrochemical cells as well.

3.1 Literature review on packaging geometry comparison

A physical and geometrical comparison of the three packaging types can be found in the work done by Lee et al. [26]. They have compared the physical constraints of jelly roll wound types (cylindrical and prismatic) with flatly stacked designs (pouch) for lithium-polymer cells. In the case of jelly roll configurations, the metal enclosure of slimmer batteries (for e.g. prismatic cells) do not exert enough pressure onto the electrodes and this results in poor thickness control. The study also enumerates some of the advantages of a flat design: uniform battery thickness, higher energy densities due to lower dead volume and lower cell impedance due to the plurality of electrical contacts through electrode tabs. Further, free stack structures without any folding options (pouch type cells) allow the separator materials to contract when exposed to shutdown temperatures. This helps in triggering safety events more easily around the electrode edges. The work illustrates the need for studying cell designs for safer lithium-ion battery technology [26].

The work by Maiser [27] gives a brief overview of battery packaging concepts, their specific advantages, and drawbacks, as well as the influence of packaging on the performance and cost. It concludes that the front-end production has the highest impact on the cost of the battery. Further, it states that back-end design and processing (packaging) adds important

safety and intelligent control features without which lithium-ion batteries would not be manageable. It also reviews a brief history, characteristics, and applications of the three packaging geometries relevant to this work [27].

Mulder et al. [28] have done a comprehensive study on the comparison of commercial lithium-ion battery technologies with different chemistries and packaging geometries. The work evaluates the behavior of these cells for automotive applications like plug-in hybrid vehicles and battery electric vehicles, where tests for high power and high energy applications are included. Within the scope of this study, commercial cells of different geometries were also studied, and a comparison was made. It was concluded that pouch cells behave better than average with respect to the power efficiency, whereas due to design factors, the prismatic shape has a clear negative effect on the efficiency. Prismatic cells also seem to have a clear negative effect on efficiency, as it becomes the hottest, while cylindrical cells warm up less. Further, pouch cells show the highest power densities. While this work is comprehensive and includes many parameters for comparison, it does not necessarily include whether the cells from the three packaging geometries have the same material and rated capacities [28]. Therefore, this work does not serve as a conclusive comparison of the three geometries.

Further literature referred for the thesis involved studies on capacity evolution, aging parameters, internal resistances and temperature rise in lithium-ion cells. The following part discusses in detail the various aspects related to capacity deterioration.

3.2 Capacity deterioration

All lithium-ion cells undergo capacity fade with time and multiple cycling. The capacity deterioration of lithium-ion cells can be studied using aging mechanisms as listed by Zhao [29]: loss of lithium inventory (LLI), loss of active material (LAM), and ohmic resistance increase (ORI). These mechanisms are discussed further in detail by González [30]. Barré et al. [31] have reviewed the aging mechanism and aging battery estimation methods in lithium-ion cells. Sarasketa-Zabala et al. [32] provide a detailed analysis of the influence of depth of discharge (DOD), C-rate and Ah-throughput on cell aging of LFP-graphite cells. Pinson [33] discusses the theory of SEI in rechargeable batteries: capacity deterioration, accelerated aging and lifetime prediction.

Most studies on understanding the aging behavior of lithium-ion cells involved tests on cylindrical cells. Han et al. [34] investigated different commercial lithium-ion cells and concluded that the aging mechanism varies with different chemistries. Two LFP-GRAPHITE cells were investigated in this study. For one cell, it was observed that the battery aging mainly arises from the loss of lithium inventory and loss of the anode active material. While

in another case, despite lithium inventory loss, no significant anode or cathode loss was observed [34]. Sun et al. [35] studied the degradation mechanism with respect to the cycle lifetime of commercial LFP-graphite cells at different ambient temperatures and observed that the mechanism changes for different temperatures. While at room temperatures, the capacity fade is due to active lithium loss by generation and reformation of SEI film, at temperatures above 35°C, the electrolyte decomposes which results in accelerated consumption of active lithium. Elevated temperatures have an adverse influence on the performance of the $LiFePO_4$ material. [35] Further, many kinds of literature have explored the use of differential voltage analysis (DVA) to study aging. In one such study, Lewerenz et al. [36] use DVA for calendar and cyclic aging of cylindrical LFP-graphite cells and focusses on mechanisms of homogeneity of active lithium distribution and loss of active anode material. They arrive at the conclusion that degradation during cyclic aging can be due to different phenomena. These phenomena can be: loss of active lithium; local loss of active anode material for DOD 100%; and deactivation of certain layers of anode and cathode due to a lithium-permeable covering layer on top of the anode. [36]

Aging has been a major topic of research for lithium-ion cells. Despite that, not much work has been done for the distinction of aging among lithium-ion cells with different packaging geometries (cylindrical cells being the most popular geometry for research). But the different mechanisms of aging have been well researched. These mechanisms are interrelated and are tailored around the SEI layer formation and changes in it. The next subsection introduces the concept of SEI layer formation, its importance for the cell aging and the different aging mechanisms.

In this thesis, the effects of high and low temperature, and high currents on the aging have also been considered. Uddin et al. [37] have summarized all the possible effects of these conditions on the cells and the results are summarized using the flowcharts in Figure 3.1.

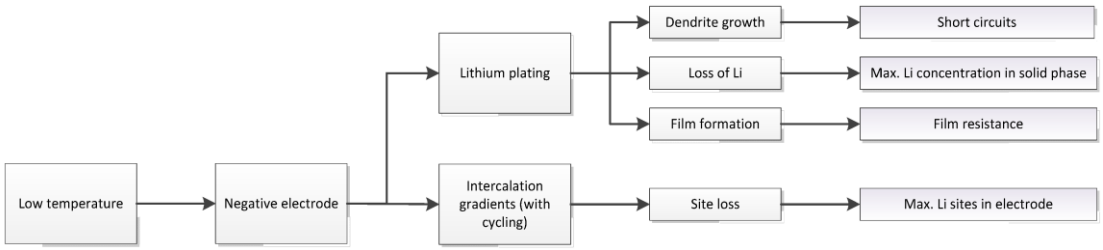

(a)

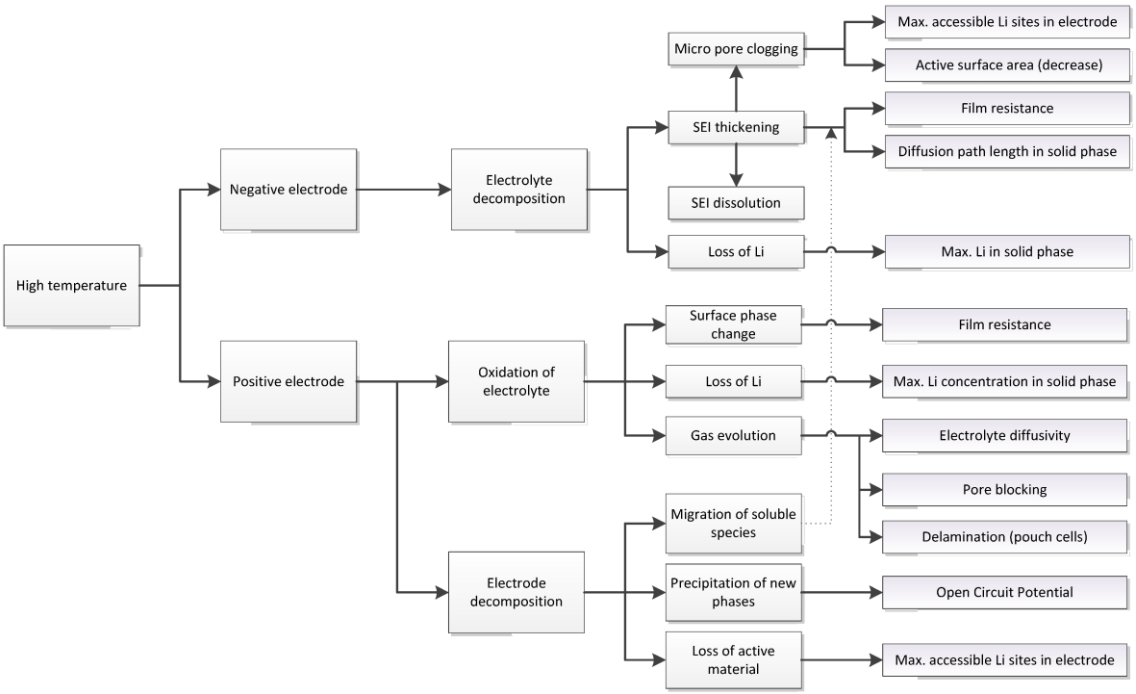

(b)

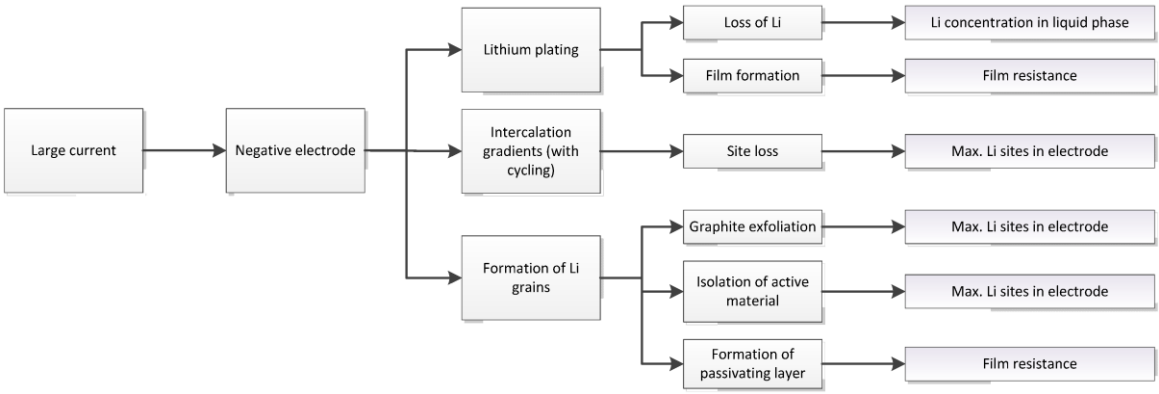

(c)

Figure 3.1. Battery degradation due to cycling at (a) low temperature, (b) high temperature, (c) large currents [37]

3.2.1 Solid electrolyte interface layer

During the first charging cycles of a lithium-ion cell, a passivation film builds on graphite/electrolyte interface. When the charging process starts, Li^+ ions transport through the electrolyte towards the graphite anode. Some Li^+ ions react with the degradation products of the electrolyte and form insoluble parts that deposit on the anode. Slow charging results in densely packed SEI layer which prevents graphite structure from decomposition [38]. Then the SEI layer strips off the solvent molecules surrounding the Li^+ ions. Additionally, the SEI layer prevents the anode lattice from exfoliation and in an ideal case, allows cycling of lithium batteries without major capacity fades (except for the initial capacity drop loss due to losing lithium inventory to SEI layer formation) [38]. It is vital to the performance of the lithium-ion cell since the entirety of the anode must have a uniform layer of SEI to prevent further electrolyte decay [26].

Xu [39] reviewed the chemical processes involved in non-aqueous electrolytes in lithium-ion batteries and also included a detailed description of SEI layer formation. It first explains passivation as the process where the products from the initial decomposition of electrolyte form a dense, protective film that covers up the pristine surface of the electrode and prevents any sustained decompositions. He also concludes from a study of other works that these passivation layers are the foundation upon which lithium-ion batteries are built. The work further goes on to discuss the formation of passivation layers on both the cathode and the anode. For simplicity of discussion, it is the passivation layer formed on the graphitic anodic layer which is widely regarded as the SEI. The study of this SEI layer on graphite is more advanced and the effects due to any changes in it are more pronounced. Xu further argues that the formation of the SEI layer is what makes the reaction within the cell reversible, by preventing consumption of both the electrolyte and more active lithium. An ideal SEI layer should be an ionic conductor and electronic insulator. [39]

The SEI layer is a mixture of lithium oxide, lithium fluoride and semi-carbonates (lithium alkyl carbonates) [39]. It depends on the composition of the organic solvents being used in the electrolyte. An et al. [40] have discussed the mechanism of SEI layer formation, shown schematically in Figure 3.2. It is generally represented in literature as a two-step process. First, the organic electrolyte components go through reduction and an isolating barrier starts forming on the graphite electrode. The reduction process takes place between 0.8 V and 0.2 V vs Li/Li^+ [40]. In the second step, the decomposition products of the electrolyte reduction undergo precipitation and the SEI layer forms until the whole graphite electrode is covered.

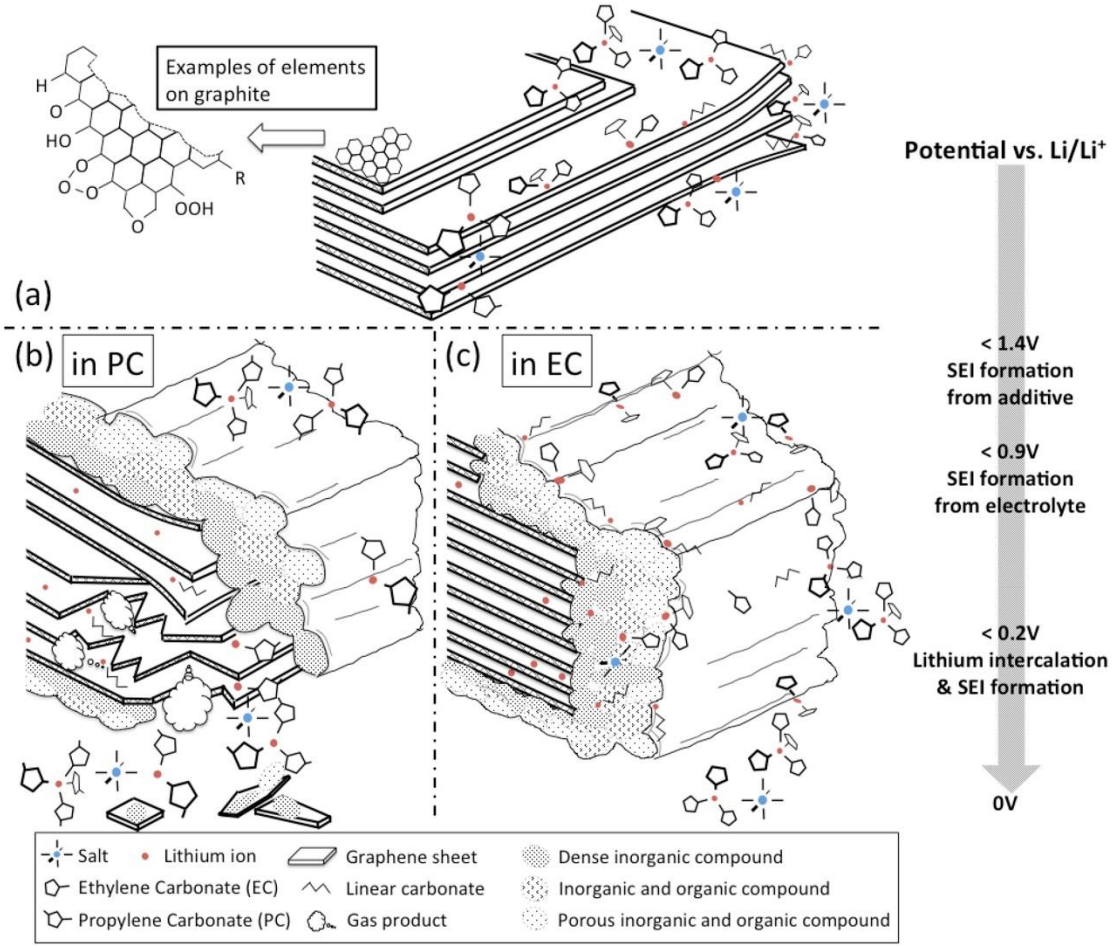

Figure 3.2. Schematic of the anode SEI formation process showing (a) graphite layers surrounded by electrolyte salts and solvents above 1.4 V vs. Li/Li^+, (b) propylene-carbonate (PC) intercalation with lithium ions into graphite layers resulting exfoliations below 0.9 V vs. Li/Li^+ and (c) stable SEI formation in ethylene-carbonate (EC)-based electrolyte below 0.9 V vs. Li/Li^+; plane side with thinner SEI and edge side with thicker SEI [40].

An optimized SEI layer is expected to have negligible electrical conductivity, high electrolyte diffusion resistance while having high lithium-ion selectivity and permeability. Once it is properly formed, further decomposition reactions with salts and solvents are prevented as electrons cannot transfer through the layers. Ideal SEI layers have high electrical resistance, high mechanical strength, tolerance to expansion and contraction stresses. [26] It should also have zero electron transference (to avoid tunneling), uniform morphology, good adhesion to carbonaceous anode surface, and low solubility in electrolytes [39].

In real cases, the SEI layer thickens gradually by repeated cycling due to electron exposure to electrolyte and electrolyte diffusion to graphite surface. Various factors can lead to further irreversible SEI layer formation consuming both electrolytes and active lithium. For example, SEI has been found to be damaged at elevated storage temperatures. This was validated by the successful detection of the reappearance of the irreversible process [39]. This not

only leads to electrolyte decomposition but also leads to the loss of active lithium [26]. The most common and fundamental source of capacity fade in optimized lithium-ion batteries (which manage to resist degradation over hundreds of cycles) is the loss of lithium to the SEI, which typically forms at the anode during recharging [33].

3.2.2 Internal resistances

In this thesis, the internal resistance has been measured from 30 s direct current (DC) pulse (charging and discharging test) which will be further discussed in the next chapter. The purpose of the pulse tests is to separate the resistances associated with different electrochemical processes during cycling at different stages of state of charge (SOC) of the cells. This sub-section includes a literature review of the different attempts at separating the resistances based on ohmic resistances and the non-ohmic resistances. It also discusses the electrochemical phenomena associated with the internal resistances. Finally, an educated approximation is made to study the internal resistances in this thesis.

A complete separation of the ohmic and non-phmic resistances of the cells are possible from a AC impedance test, as discussed by Zhang Zhou et al. [41]. They have studied different dynamic phenomena inside the battery: lithium-ion migration through the SEI layer, activation kinetics in both negative and positive electrodes, double layer effects at the interfaces of electrolytes, and lithium-ion diffusion processes in the active material of the electrodes. The resistances related to the various sections of the reaction cell are studied by performing the electrochemical impedance spectroscopy (EIS). This can be explained using the Figure 3.3. The different regions correspond to different internal resistances and chemical phenomena. Region A can be represented by single ohmic resistance, R_o, and includes resistances of the current collector, active material, electrolyte and separator. Region B represents the SEI layer resistance (R_{sei}) – characterized by a high frequency. Region C (medium frequency) represents the charge transfer resistance (R_{ct}). The low frequency region, D, represents the lithium-ion diffusion process in the active material of the electrodes [41].

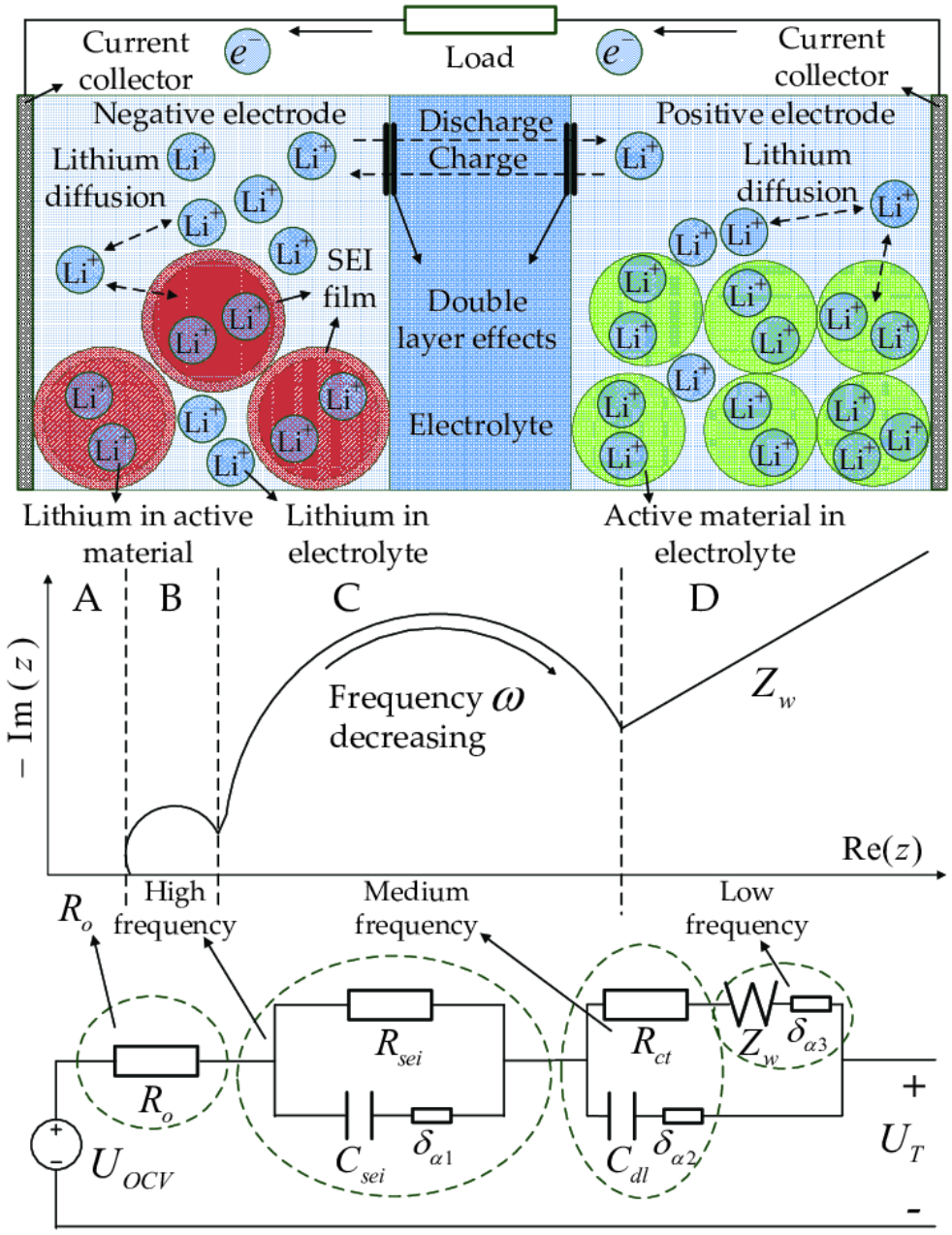

Figure 3.3. Lithium-ion cell internal dynamics and equivalent impedance circuit [41]

Compared to AC pulse based EIS method, the DC pulse test can only provide a general approximation to separate the ohmic and non-ohmic parts. This is explained in the work done by Barai et al. [42]. They have studied the effect of measurement time-scales on DC internal resistance measurement. Figure 3.4 shows a schematic of a cell voltage response to a pulse current. Based on the timescales, the voltage drop phenomena can be differentiated as [42]:

- the instantaneous voltage drop is due to the pure ohmic resistance (R_o) which comprises all electronic resistances and the bulk electrolyte ionic resistance of the battery, as shown in Table 3.1.

- the potential drop within the first few seconds is due to the battery's double layer capacitance and charge transfer resistance (R_{ct}) which is attributed to the charge transfer reaction at the electrode/electrolyte interface
- the shallow, linear (or close to linear) voltage drop is due to polarization resistance (R_p) which accounts for ionic diffusion in the solid phase and is usually considered to be the rate-determining step for lithium-ion cells

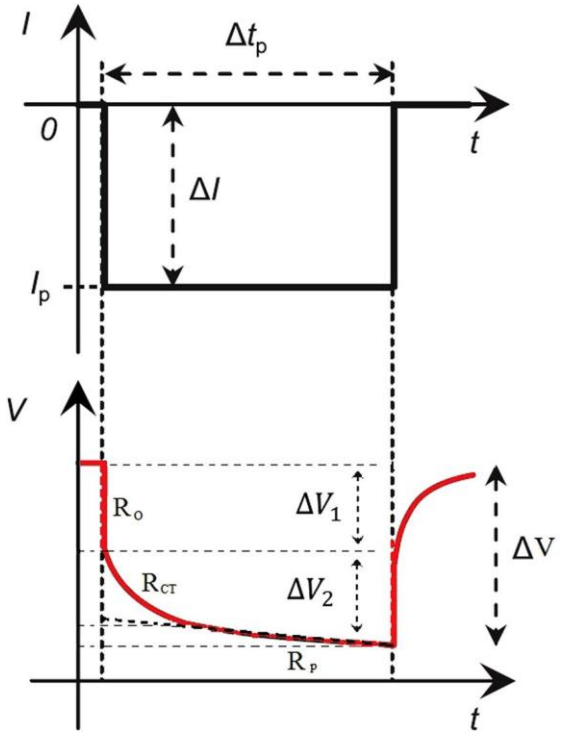

Figure 3.4. Schematic to show cell voltage response to a pulse current. [42]

The electrochemical behavior of the cells in this thesis is discussed using the DC pulse test, where the measured internal resistances have both the ohmic and non-ohmic components. The approximation done by Barrai et al. [42] is used to study these resistances. For secondary or rechargeable cells like lithium-ion cells, these parameters differ greatly from one SOC value to other (i.e. the capacity contained in the cell at that instant), therefore, the pulse test is done at different SOC steps. A drawback of DC pulse test to obtain resistances is that it shows only the imposition of all the different contributions to resistance. Therefore, it cannot completely separate the different resistance components [42].

Table 3.1. Components of internal ohmic resistances [43]

Components of ohmic resistance	**The internal ohmic resistance of the cell, R_i=ionic resistance + electrical resistance + interfacial resistance**
Ionic	• Electrode particle • Electrolyte
Electrical	• Electrode particle • Conductive additives • Percolation network of additives in the electrode • Current collectors • Electrical taps
Interfacial	• Between electrolyte and electrodes • Between electrode particles and conductive additives • Between electrode and current collectors • Between conductive additives and current collectors

3.2.3 Aging mechanisms

During aging, the cell undergoes structural or chemical change that may lead to changes in properties like energy throughput, capacity etc. Cell degradation can be slow due to gradual deterioration and gradual performance loss. It could also be due to sudden catastrophic damage due to thermal runaway or short circuit [44]. The aging mechanism in the cathode and anode are different because of their different materials. The cell aging is not uniform and depends on many factors as discussed in this section. These can also be explained by using different aging mechanisms.

Aging of the anode electrode results in modification of graphite anode with time and use [45]. The importance of the SEI layer in a lithium ion cell has been discussed already. One of the aging mechanism in the anode is related to changes or damage to this SEI layer. In the long-term cycling, the SEI layer can penetrate the pores of the electrode materials and

separators. This may result in reduced accessibility of the active surface area [44]. Further, high temperatures can lead to breakdown of the SEI layer. This leads to reformation of the SEI layer by consumption of the cyclable Li^+ ions [45]. Low temperatures can lead to the phenomena called lithium plating which is explained later in this subsection. Lithium plating leads to further consumption of cyclable Li^+ ions.

Aging mechanisms in cathode materials can originate from structural changes, phase transition in the active material, electrolyte decomposition, dissolution of metal oxide, and secondary reactions such as current-collector corrosion and binder decomposition [44]. The intercalation-deintercalation of Li^+ ions induce mechanical stresses and strain in the active material. It could also cause phase transitions which are not 100% reversible processes [44]. Figure 3.5 shows diagrammatically the possible aging mechanisms in the cathode.

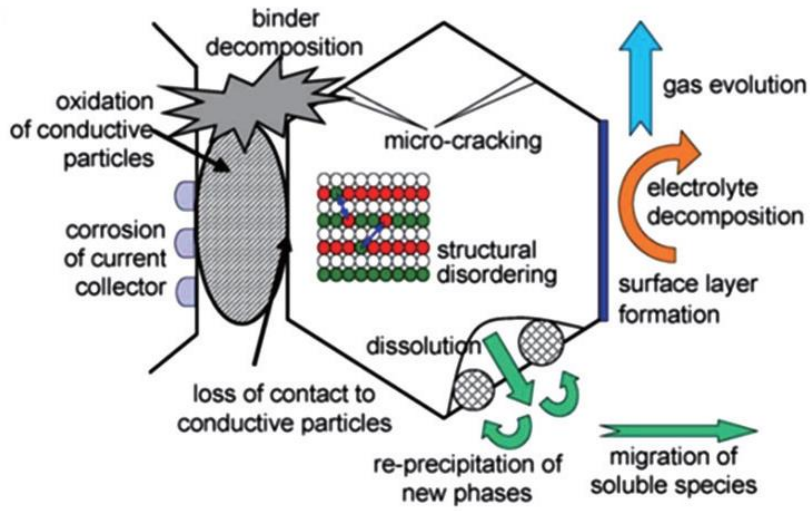

Figure 3.5. Schematic showing cathode aging mechanisms [45]

Arunachala [44] has summarized the effect of different stress factors on the aging of the electrodes as depicted in Table 3.2.

Table 3.2. Stress factors influencing Lithium-ion cell aging mechanism [44]

Stress factor	**Aging mechanism**	**Causes and effects**
Temperature	Cathode degradation	Increase in charge transfer resistance
	SEI Layer	Unstable SEI, increase in overpotential
	Anode degradation	Decomposition and irreversible reactions
	Electrolyte decomposition	Cell impedance increase
	Active Li^+ ions	Accelerates the irreversible SEI formation
Voltage/SOC	Electrolyte decomposition	SEI growth, loss of Li^+, electrolyte unstable
	Loss of active Li+	SEI layer restricts ionic conductivity
Time	SEI formation	SEI grows over time
	Electrolyte decomposition	Capacity fade and impedance loss
	Loss of active Li^+	Increases side reactions
ΔSOC	Side reactions	Loss of active Li^+ with time
	Volume expansion	Mechanical stress and damage to anode
Cycles	Side reactions	Anode degradation
	Phase transitions	Destabilization of cathode structure
Discharge rate	Anode degradation	SEI degradation and reformation
	Electrolyte decomposition	Anode stability affected by side reactions
	Interfacial resistance	Slow diffusion, internal resistance increase
Charge rate	Side reactions	Lithium plating and dendrite growth

The aging process of lithium-ion cells is a complex process. There is no standard formula to explain it. Different mechanisms apply to different cells and conditions. But for the ease of study in this thesis, three aging mechanisms, as shown by Zhao [29] and Gonzalez [30], have been considered: loss of lithium inventory, loss of active material and ohmic resistance increase.

LLI leads to loss of lithium ions due to parasitic reactions, though it does not change the chemical composition of active materials in electrodes and their properties. It is reported to be the major cause of degradation of lithium-ion cells. It is attributed to two main causes: the primary cause is the SEI layer formation, growth, and destabilization. LLI occurs chiefly at the electrode/electrolyte interface and is predominant on the anode where SEI formation dominates. SEI growth and subsequent LLI is dependent on temperature. At high temperatures, the SEI either grows in thickness or becomes non-protective leading to performance degradation, whereas at low temperatures, the risk of lithium plating leads to cell damage [30]. Low temperatures slow down Li^+-diffusion into anode, which compounded with operating voltage close to lithium metal, leads to metallic lithium plating on the anode surface. Lithium plating occurs during charging when lithium-ions deposit on the anode instead of intercalating into the graphite. This is shown in Figure 3.6. The process continues and forms lithium dendrites during charging. Lithium dendrites subsequently react with electrolyte to accelerate the aging process or in the worst case, cause an internal short circuit. could be hazardous as it is associated with safety issues [44]. It is initiated by strenuous charges, charging at low temperatures, cell constructive design or conventional aging of the cell. It can also result from operating at low temperatures and high charge current rates) [30].

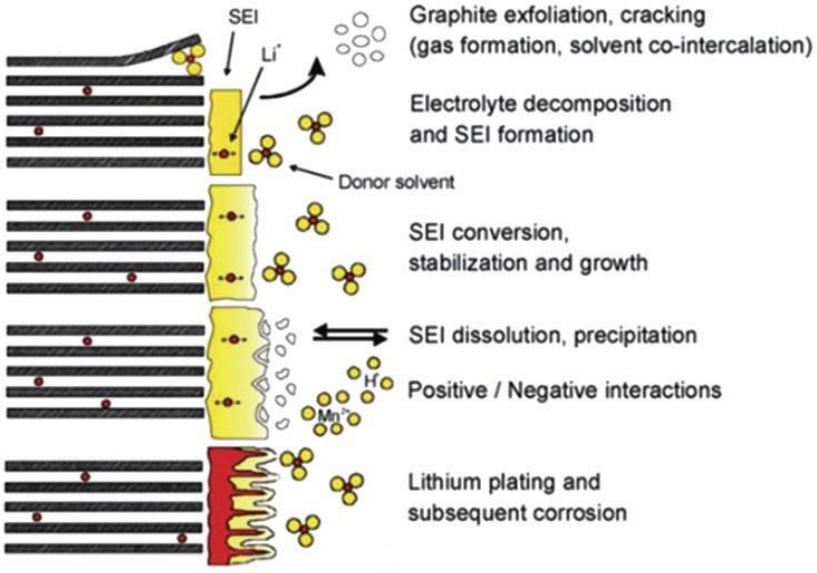

Figure 3.6. Schematic showing the SEI and graphite anode under normal conditions and under the influence of lithium plating [45]

LAM directly affects the structure of the electrodes, reducing the amount of active material used in the cell. The aging effects due to LAM are more prominent in graphite-anodes than in cathodes. It is enhanced by high currents, high temperatures, and high SOC. The major reasons for LAM are particle isolation, side reactions within the active material of the electrodes and the electrolyte-electrode interface. LAM may lead to second stages of cell degradation where abrupt capacity losses might appear after a steady capacity loss in the first stage [30].

In ORI, degradation caused on the electrodes and electrolyte materials directly result in the increase in the electronic and ionic resistances, respectively. The possible reasons for ORI are particle isolation causing LAM, binder decomposition, current collector corrosion, volume changes in active material and electrolyte contamination, and SEI growth and destabilization affecting ionic resistance [30]. The ohmic and non-ohmic resistances are separated and studied in detail in section 3.2.3.

This chapter served to understand the underlying theory behind the work done in the thesis. It started with a literature review of the studies on packaging geometries. Then the formation and importance of the SEI layer was studied. In the next part, the methods to separate the ohmic and non-ohmic components of resistances were studied and adapted into the thesis. Further, the different factors affecting aging and aging mechanisms were summarized. The next chapter discusses the specifics of the cells manufactured and moves on to the experiments performed on the cells within the scope of the thesis.

4 Experimental Setup

This chapter discusses the conditions and methods for the manufacture of the cells along with the cell testing. In the first part, the cell geometry, size and chemical composition of the cathodes and anodes are mentioned. The second part describes the test performed on the cells which are used within the scope of this thesis.

4.1 Cell chemistry

To have a common comparison standard between the cell packaging geometries, the chemistry for the anode, cathode, electrolyte, and separator were chosen to be the same. All cells manufactured have the same materials for the electrodes, $LiFePO_4$ as the cathode and graphite as the anode. Both the materials of the electrodes are from the same batch of raw materials for all the cells [46].

The separator used for the cell manufacture is a tri-layer Celgard 2325 grade [46]. This type of tri-layered poly-olefin separator consists of 1 polyethylene (PE) layer sandwiched between two layers of polypropylene (PP) and is the most commonly used separator type. This is because of their chemical inertia and the safety feature the combination of PP-PE-PP offers. In the case of overheating, the PE layer melts, losing its porosity (i.e., mechanically blocking the Li^+ ion movement), while the PP layer prevents large dimensional changes until its own melting, thus preventing short-circuits.

The composition of the electrolyte solution strongly influences the temperature dependence of the capacity. This is related to the quality of the passivation of the graphite electrodes in the various solutions and to the transport properties of the passivating surface films that cover the graphite particles (discussion related to SEI layer formation). [47] For the cells manufactured by SPICY, the electrolyte solution used is a blend of ethylene carbonate (EC), propylene carbonate (PC) and dimethyl carbonate (DMC) in volume proportion 1:1:3, respectively, with 1M of $LiPF_6$ and 2% weight of vinylene carbonate (VC) [46].

4.2 Cell geometry and size

The three packaging geometries (cylindrical, prismatic and pouch) were assembled in different ways (as shown in Figure 2.5), which are mentioned in the SPICY Deliverable 5.6 [46].

Jelly roll manufacturing was used to wind the electrodes and separator in cylindrical and flat cores for cylindrical and prismatic cells, respectively. While the cylindrical cores are basically rolls of electrodes with separators within them, for the prismatic cells, the cores resemble

layers placed into a Z-shape. Next, the cells are welded together complete with the placing the current collectors and finally welding the top cap. The electrolyte is filled using different holders through the aperture at the top cap. It is necessary to ensure that the electrolyte solution covers every pore in the internal structure and the separator membrane. After this step, the cells are conditioned outside the dry room.

The pouch cells were manufactured separately. The process lacked a standardized equipment and therefore, needed some manual work initially. In the first step, the electrodes and the separators were cut into layers using a cutting press and stacked into layers of 38 anodes, 76 separators and 37 cathodes. The terminals were drawn out and tabs were welded on them. The stacks thus formed were wrapped in two half-aluminum shells and heat sealed. The pouch cells were filled with the electrolyte solution in a glove box and the remaining side was welded. Then the cells were conditioned outside the dry room and the trapped gas bubbles in the structure were degassed as the last step. The three cell geometries manufactured are shown in Figure 4.1. The cell specifications of each geometry are mentioned in Table 4.1.

(a) (b)

Figure 4.1. Cells manufactured (a) Prismatic (L), Cylindrical (R), (b) Pouch [46]

Table 4.1. Cell specification for cells of different geometries [44]

	Cylindrical	**Prismatic**	**Pouch**
Lower Voltage limit (V)	2.5	2.5	2.5
Upper Voltage limit (V)	3.6	3.6	3.6
Max charge current (A)	50	4	50
Max discharge current (A)	100[1]	4[2]	100[3]
Temperature range (°C)	[-10, +55][4]	[0, +45]	[-10, +55][5]
Energy density (Wh/kg)[6]	108.61	94.25	121.77
Capacity (Ah)	16.099	15.963	14.889
Weight (g)	474.32	541.98	391.25
Height (mm)	125	125	-
Surface area (mm²)	19625[7]	31250[8]	-

A mass analysis was done for all the cells and the average weight contribution of the different components of each cell are shown in Figure 4.2. A clear difference is noticed in the cells with soft packaging, i.e. the pouch cells, due to the softer casing.

[1] for a 30 s pulse

[2] normal cycling, rate tests up to 12 A

[3] for a 30 s pulse

[4] for charging [+5, +55]

[5] for charging [+5, +55]

[6] Energy density, $E = \frac{Q \times V_{nom}}{m}$, where Q = Capacity, V_{nom} = nominal voltage, m = mass

[7] Curved surface area of cylindrical cell = $2\pi rh$

[8] Curved surface area of prismatic cell, considered to be cuboidal = $2(l + b)h$

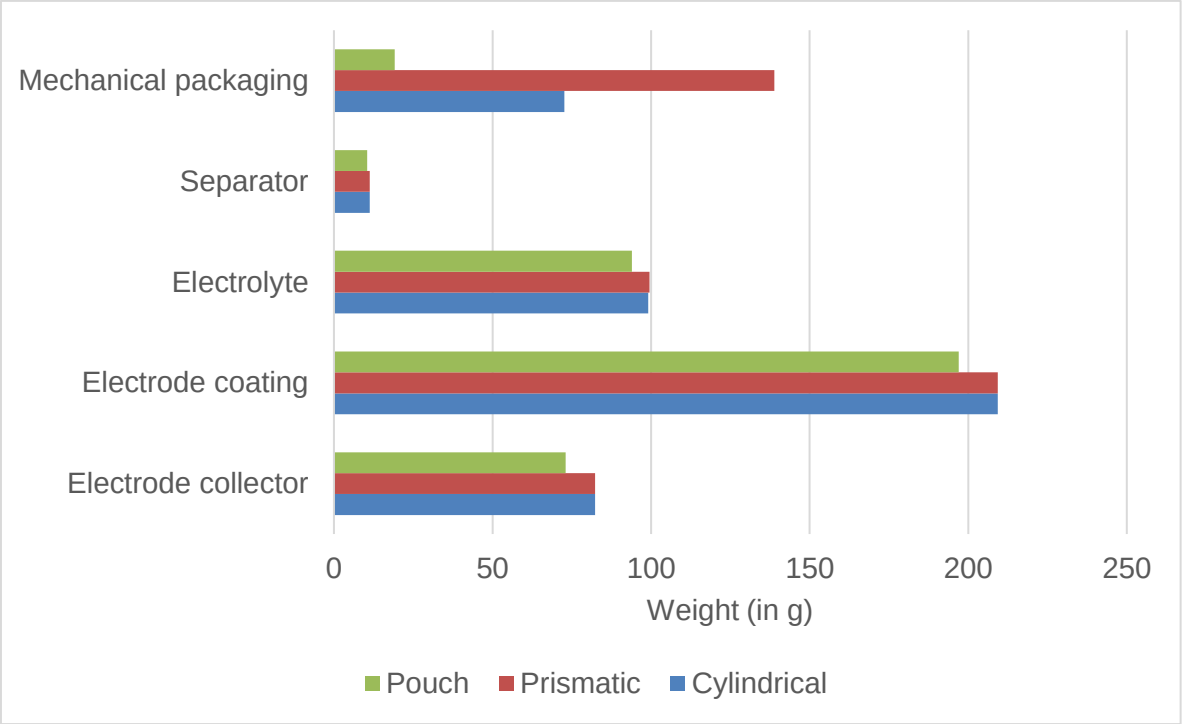

Figure 4.2. Weight analysis of the cells. [46]

The mass analysis is as expected because of the hard cover being replaced by aluminum foil in the pouch cells, reducing the weight of the packaging component. In the case of the prismatic cell, it requires more packaging than a cylindrical cell because of the higher surface area, as can be seen from the reception test data given in Table 4.1.

The data presented above were measured without any aging. After the reception tests, the cells were aged and cycled at different stages of state of health (SOH). The following subsection explains the different tests performed relevant to the current work.

4.3 Tests performed

Within the scope of this thesis, only the life cycling tests have been included. It involves testing of the cells at different charging/discharging rates at different conditions of temperature over different SOH or aging time. In the cycle tests, the equivalent full cycles are observed over the aging of the cells.

All the cyclic life tests involve two kinds of checks – short check-up (SCU) and extended check-up (ECU). The ECUs involve the measurements of capacity evolution, open circuit voltages (OCV) and internal resistances by pulse tests. Another test involves the temperature developed at the first ECU for different charging and discharging rates. Within the scope of this thesis, the capacity evolution, the internal resistance developed in different capacities (pulse tests) and the temperature is the most interesting.

The life-cycle test standards are documented in SPICY Deliverable 6.1 [48]. The usual test conditions as mentioned in this deliverable can be enumerated as follows [48]:

i. The SOC calculated is the capacity calculated at a usual discharge rate of 1C at 25°C.
ii. The SOH refers only to the battery capacity decrease.
iii. The usual test conditions of C-rates for charging are 1C, 2C, whereas for discharging are 0.2C, 0.5C, 1C, 2C
iv. For this work, the SOC window for cycling is 0% to 100%
v. The end of life (EOL) is set to 80% of initial capacity and most test results in this work contains values for a minimum SOC of around 80%.

The following subsections cover the tests performed on the cells which are relevant within the course of the work.

4.3.1 Capacity evolution of the cells

This test is performed to determine the cell deterioration or capacity loss. Of special interest is the capacity deterioration over the possible number of equivalent full cycles (EFC). The capacity deterioration is measured as SOH drop.

As mentioned earlier in the discussion of the test conditions, the SOH refers only to the battery capacity decrease. The SOH is not a well-defined physical quantity. It can be defined and determined by using any measurable quantity that changes with aging of the cell for example capacity, internal resistance, cell impedance, cycling temperature gradient changes etc., and is monitored with respect to the values for a new cell. Therefore, such details are not provided by the manufacturers and must be independently determined by the testing infrastructure. There is no precise definition of SOH agreed upon uniformly by industries or scientists [49]. The SOH estimation within this work, as mentioned, has been done by measuring changes in the capacity of a fully charged cell.

For this work, the charge-discharge cycling method and the subsequent SOH calculation is described below with the help of Figure 4.3. The figure shows a sample plot taken from a test on a cylindrical cylinder. It shows the instantaneous capacity and the current profiles for charging and discharging. It helps in explaining the SOH estimation as shown further. The cells were charged and discharged using the conventional constant current-constant voltage (CC+CV) protocol [50]. It involves a low rate constant current charging to a predefined cut-off voltage followed by float charging at the cut-off voltage until the current drops to very low preset value. The positive current and instantaneous capacities are for charging, while the negative values depict discharging.

i. An unaged cell is fully discharged, and the residual capacity is measured and noted.

ii. Next, the cell is charged again first with constant current (CC) and then with constant current + constant voltage (CC+CV). When the cell is fully charged, the capacity is measured again and noted.

iii. This fully charged cell is discharged again and another discharge cycle, as described in step ii above, is carried out.

iv. The cell is charged a second time and the cell capacity after the second discharge is noted and labeled as the $Q_{reference}$ (reference initial capacity) of the unaged cell. This corresponds to the capacity at 100% SOH.

v. Steps i through iv are repeated for the aged cell and the cell capacity after the second discharge-charging cycle is noted and saved as $Q_{i,aged}$ (the capacity of the aged cell at the ith step). The SOH of the aged cell is calculated using the equation (4.1):

$$SOH_i = \frac{Q_{i,aged}}{Q_{reference}} \times 100 \tag{4.1}$$

where, SOH_i is the state of health at the ith step

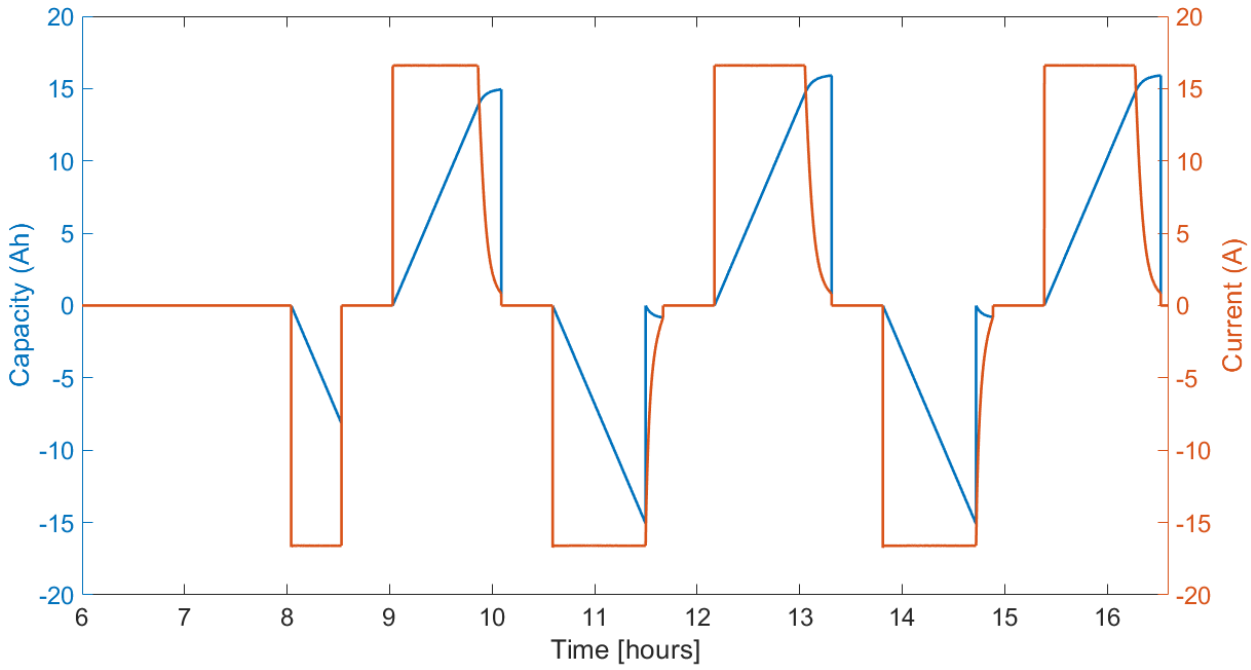

Figure 4.3. A sample plot to show the capacity evolution for the calculation of SOH

An aged cell has reduced full capacity and the number of full cycles it has gone through its life is not a linear curve with linear multiplicity. This quantity is defined by the term EFC. The EFC can be calculated using the equation (4.2) [51]:

$$N_{eq} = \frac{W_{tot}}{2 \times U_{nom} \times Q_{init}} \tag{4.2}$$

Here, N_{eq} = equivalent full cycles, W_{tot} = accumulated energy throughput for the cycled cell, U_{nom} = specified nominal battery voltage, Q_{init} = measured initial battery capacity

The capacity evolution or deterioration is studied with respect to changes in SOH and EFC. These conditions are checked for the cells of the three geometries for different conditions of temperature and cycling current rates. These results are discussed in the next chapter.

4.3.2 Temperature developed over cycling

To determine the temperature gradient over the three geometries at similar conditions, the temperatures were measured for the first ECU cycle with different cycling current rates. In all the cases, the charging was done with a rate 1C, but the discharging was tested with slow to faster C-rates.

The temperature sensors used for the tests were the negative temperature coefficient (NTC) sensors. This is the most commonly used type of temperature sensors, and in this case, the temperature shows an inverse relationship with respect to the resistance. NTC thermistors are high precision and can give a resolution and accuracy as low as 5 mK [52]. The different stages of the charging and discharging were identified by using the data for the cell voltage.

In all the experiments performed on the cells, the SOC have been provided in the test plans. The most common way of measuring and keeping tracking of the SOC is the coulomb counting method. In this method, the discharging current, $I(t)$, of a battery is measured and integrated over time to estimate SOC as shown by the equation (4.3) [53]:

$$SOC_t = SOC_0 - \frac{\int_0^t I(t)dt}{Q_n} \tag{4.3}$$

where, Q_n is the nominal capacity measured in the beginning of cycling, and t is the time at which the SOC_t needs to be calculated with respect to the initial SOC_0.

4.3.3 Direct current pulse test

In this work, the internal resistance has been calculated for 30 s charge and discharge pulses at the 0.5 s, 10 s and 30 s time-instants. This section discusses the experimental procedure for the same.

Two types of pulses are used during the test: one for increasing the SOC and another 30 s pulse for measuring the internal resistance. While charging, first the SOC is determined for a fully discharged cell and a pulse of 1C is applied for the 30 s at that SOC. Next, the cell stabilizes for a while without a pulse and then it is charged again at 1C this time to increase its SOC. In the case of discharging, the only difference is that a current is drawn from the cell. This is explained using Figure 4.4.

This method is used for the SOCs: 5%, 10%, 20%, 30%, 40%, 50%, 60%, 70%, 80, 90% and 95%. Further, for each 30 s pulse, the internal resistance is calculated at the 0.5 s, the 10 s, and 30 s instant. This is done by calculating the instantaneous change of voltage in and dividing it by the current at that time in Figure 4.4 (which is approximately equal to 1C), as shown in the equation (4.4):

$$R = \frac{dV}{dI} = \frac{V_2 - V_1}{I_2 - I_1} \tag{4.4}$$

Where, ∂V refers to the change in voltage from initial voltage, V_1, at the start of the pulse to the voltage, V_2, at the point of measurement in Figure 4.4. Similarly, dI refers to the change in current value from I_1 to I_2

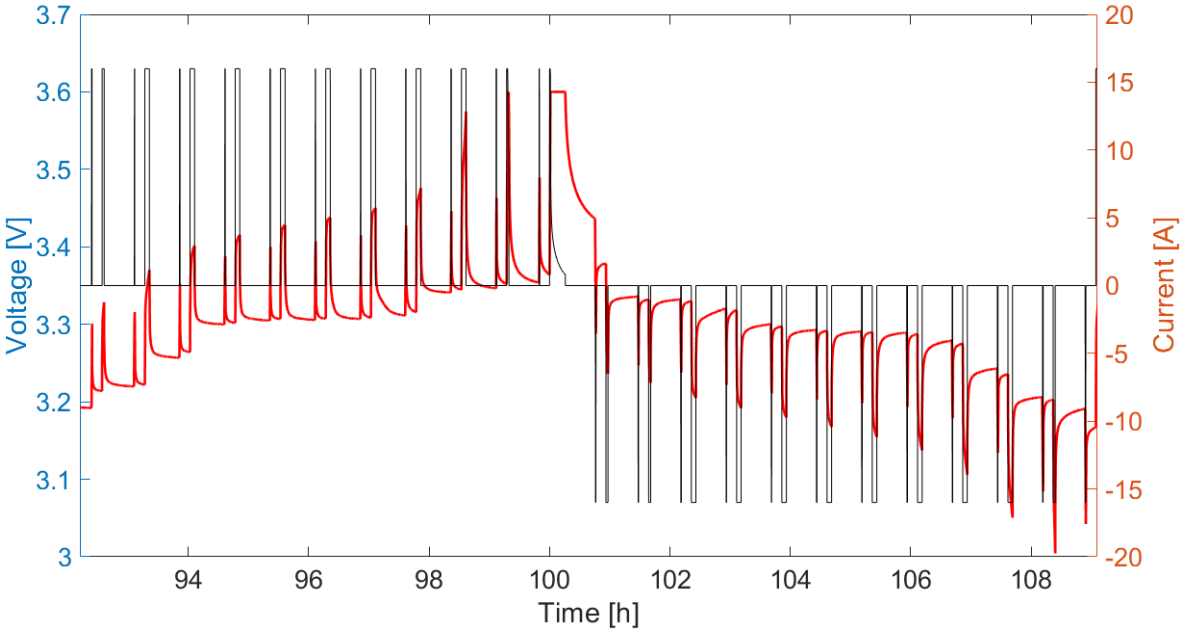

Figure 4.4. The explanation of a 30 s pulse test with current pulses and voltage evolution

5 Results and Discussion

The MATLAB Data Processing and Visualization tool is used to extract, sort, edit and visualize the experimental data for analysis. It is found that the data for cells under the same conditions of cycling rate and temperature show similar results and therefore the cell data were averaged. Further, in certain cases, data interpolation and extrapolation are used to maintain uniformity. The following subsections discuss the experiment results from the previous chapter along with any assumptions made in each case.

5.1 Reception test data discussion

The study of the cell chemistry and materials shows the measured values for parameters like cell weights, capacity, and energy densities. As discussed, a possible reason for the lower weight of the pouch cells is due to its light-weight aluminum pouch cover and lack of any hard covering. A mass analysis of the different components of the cells is also done in Figure 4.2. The difference in the weights of the prismatic (heavier) and cylindrical cells can be explained using the higher surface area of cover for the case of the prismatic cells. This leads to the higher requirement of metallic cover material. The added mass in the case of the prismatic cells can also be attributed to an added metallic/steel support for stability. [27] In a pouch cell, the cathode, separators, and anode are stacked in layers, as can be seen in Figure 2.5. This approach increases packaging density to the maximum and saves weight, thus increasing the energy density of the cell. The packaging density of cylindrical cells is low due to their round shape and the cell case is comparatively heavy. [27]

Due to the weight comparisons as discussed, it is not surprising that energy density (Wh/kg) of pouch cells is the highest followed by cylindrical cells followed by prismatic cells. (Considering that all the cells have a capacity close to 16 Ah).

While all the cells have been manufactured to be around 16 Ah, Table 4.1 shows a minor difference in the capacities of the cells. (Cylindrical = 16.099 Ah, Prismatic = 15.963 Ah, Pouch = 14.889 Ah). While cylindrical and prismatic cells are almost equal to 16 Ah (cylindrical slightly higher), the capacity of pouch cell is slightly below 15 Ah. Figure 4.2 can provide a possible reason for it. It shows that mass of the electrode collector + electrode coating + electrolyte material is clearly less in the case of pouch cells as compared to prismatic and cylindrical geometries. The less electrode + electrolyte content in pouch cells might explain the reduced capacity.

The next sections discuss first the performance of a new unaged cell with respect to internal resistance profiles from the pulse test and then the temperature evolution over cycling of

each geometry. The section after that discusses the effect of aging on the cells, namely, the capacity deterioration and EFCs at different conditions of temperature and cycling, and the influence of aging on internal resistances. For ease of study and data representation, all the data values for the same geometry and same test conditions are averaged out.

5.2 Performance of unaged cells

The data obtained from the tests are pre-processed by averaging the values for the same geometry and same test conditions (C-rate and temperature). For simplicity, only the data for the 0.3C-rate condition are considered.

5.2.1 Internal resistance of unaged cells

The unaged cells are subjected to the 30 s DC pulse test as explained in the section 4.3.3. The internal resistances are calculated at different SOCs.

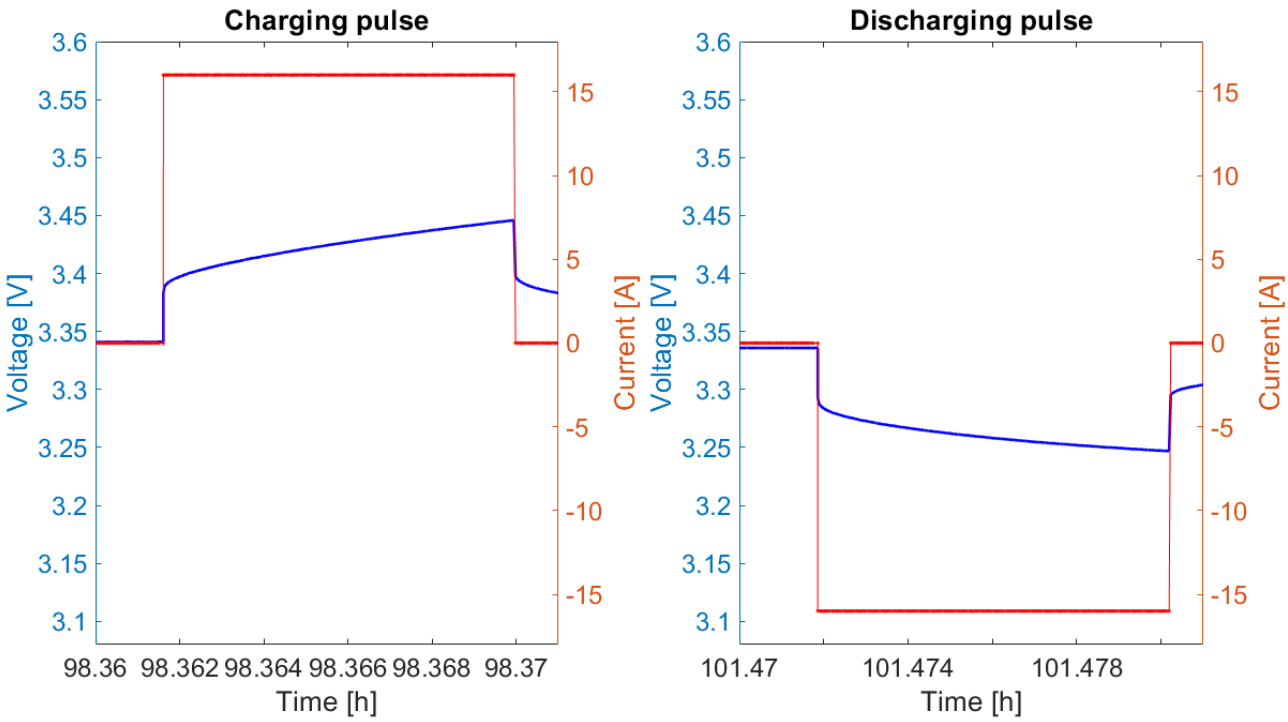

Figure 5.1. Sample current and voltages curves for 30 s charge and discharge pulse

Figure 5.1 depicts sample current and potential drop curves for 30 s charge and discharge pulses. The sample data is taken from a test done on a cylindrical cell for a particular SOC. Figure 5.1 resembles the schematic depicted in Figure 3.4 which shows a schematic of a cell voltage response to discharging pulses. Due to this coherence, the resistances measured by the 30 s DC pulse test can be depicted using the literature studied in section 3.2.2.

In this thesis, the internal resistances for each SOC are measured for the 0.5 s, 10 s and the 30 s instants. These time instants can be used to represent different phenomena within the cell function. The 0.5 s resistance is approximated to represent the ohmic resistance. The 10 s instant also includes the charge transfer reaction at the electrode-electrolyte interface and the Li^+-electrolyte concentration gradient formation (lithium-ion mass transport phenomena). The 30 s instant can be approximated to represent all resistance components including the lithium-ion diffusion. This is summarized in Table 5.1.

Table 5.1. Characterizing the ohmic and non-ohmic resistance components with time instants of 30 s DC pulse tests

Time instant of the calculated resistance	**What the resistance represents**
0.5th s instant	Ohmic resistance
10th s instant	Ohmic resistance + charge transfer kinetic resistance
30th s instant	Ohmic resistance + charge transfer kinetic polarization resistance + Diffusion polarization resistance

The resulting data comparison between the different cell geometries is represented in Figure 5.2 and Figure 5.3. The first observation from the curves is the low internal resistance in pouch cells in general as compared to the other two geometries. This is expected because of the thin electrode slices used to stack together in pouch cells. Thinner the electrodes, smaller is the transport path for the ions, and therefore, lesser the internal resistance. Though it is interesting to note that the internal resistance in pouch cell is higher at the extreme ends of the SOC, that is, at 0% and 100%. A slight increase in internal resistance is also observed for all geometries around the 60-70% SOC range.

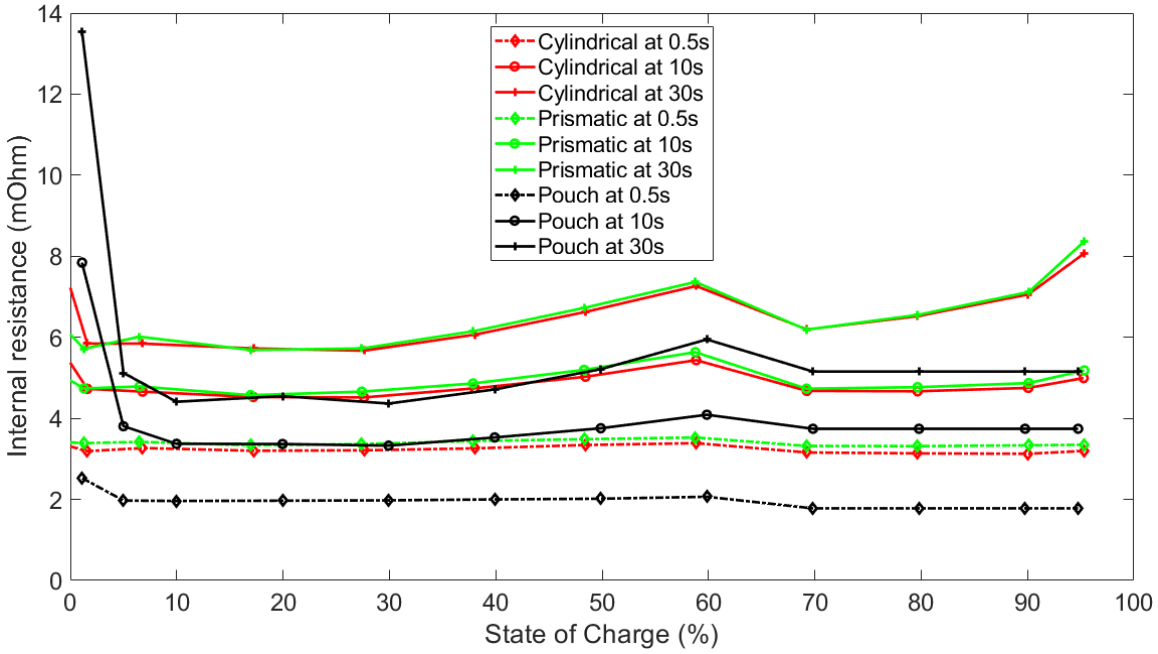

Figure 5.2. Internal resistance comparison for a charging pulse

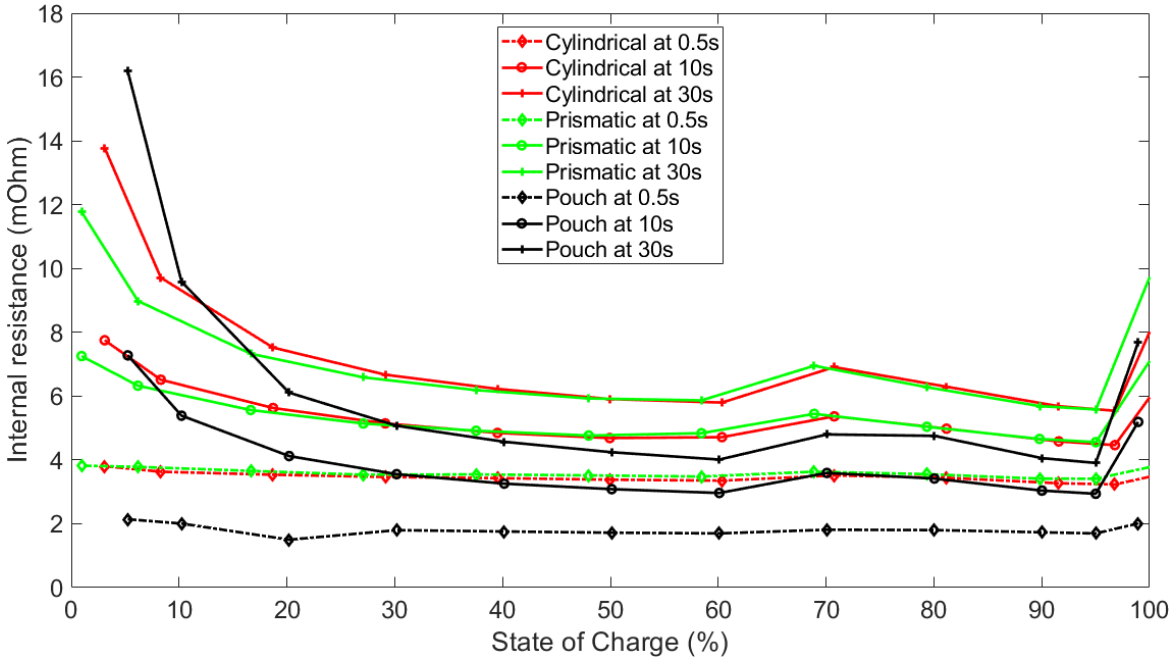

Figure 5.3. Internal resistance comparison for discharging pulse

For convenience, internal resistance values from the curves above are documented for SOCs of 5%, 50% and 95% in Table 5.2.

Table 5.2. Internal resistance at selected SOCs for charging and discharging pulses (time instant based)

	5% (in mOhm)			**50% (in mOhm)**			**95% (in mOhm)**		
Pulse in-stant	***0.5 s***	***10 s***	***30 s***	***0.5 s***	***10 s***	***30 s***	***0.5 s***	***10 s***	***30 s***
Charging pulse for cells at 5°C/0.3C									
Cylindrical	3.24	4.68	5.84	3.34	5.03	6.63	3.20	4.99	8.06
Prismatic	3.41	4.77	5.93	3.49	5.20	6.73	3.35	5.18	8.37
Pouch	1.97	3.81	5.12	2.02	3.76	5.21	1.78	3.74	5.15
Discharging pulse for cells at 5°C/0.3C									
Cylindrical	3.74	7.30	12.29	3.38	4.69	5.91	3.22	4.45	5.53
Prismatic	3.79	6.54	9.62	3.52	4.76	5.93	3.41	4.56	5.58
Pouch	2.14	7.28	16.19	1.72	3.08	4.24	1.70	2.94	3.91

The resistances can be further classified into the ohmic and non-ohmic components as shown in Table 5.3. As discussed in previous chapters, the DC pulse test does not give an accurate estimation of the individual ohmic and non-ohmic resistances. For example, the pure ohmic resistance needs to be ideally measured instantaneously after the pulse starts. The 0.5th second already has charge transfer kinetic components included in the resistance. But for simplicity, the 0.5th second resistance is approximated to be the ohmic (Ohm) resistance. The difference between the 10th second resistance and the 0.5th second resistance is approximately the charge transfer kinetic (CTK) resistance. The difference between the 30th second resistance and the 10th second resistance is approximated to be the diffusion polarization (Dif) resistance.

Table 5.3. Table showing the ohmic and non-ohmic resistances at selected SOCs

	5% (in mOhm)			50% (in mOhm)			95% (in mOhm)		
Pulse instant	***Ohm***	***CTK***	***Dif***	***Ohm***	***CTK***	***Dif***	***Ohm***	***CTK***	***Dif***
Charging pulse for cells at 5°C/0.3C									
Cylindrical	3.24	1.44	1.16	3.34	1.68	1.60	3.20	1.80	3.06
Prismatic	3.41	1.36	1.16	3.49	1.71	1.53	3.35	1.83	3.18
Pouch	1.97	1.83	1.32	2.02	1.74	1.46	1.78	1.96	1.41
Discharging pulse for cells at 5°C/0.3C									
Cylindrical	3.74	3.56	4.99	3.38	1.30	1.22	3.22	1.23	1.07
Prismatic	3.79	2.75	3.08	3.52	1.25	1.16	3.41	1.15	1.02
Pouch	2.14	5.14	8.91	1.72	1.36	1.16	1.70	1.24	0.97

As discussed above, 0.5 s values can be approximated to represent the ohmic resistance comprising all the electronic and bulk ionic resistance. Ideally, the ohmic resistance calculated must be the instantaneous resistance calculated at the onset of the pulse, but this is limited by the measuring instrument's data acquisition capacity [42]. The ohmic resistance of pouch cells are in general the least for all conditions of SOC while it is the highest for prismatic cells. The 0.5 s instant resistances or the faster dynamic effects are relatively uniform over the entire SOC range, both for the cases of charge and discharge. Higher the electrode potential, the harder it is to remove a lithium from a site within the host matrix [54]. On discharging a cell, lithium is transferred from a high energy state in the anode to a low energy configuration in the cathode, hence, the resistance values for discharging should be higher than that of charging [42]. As shown in the values in Table 5.2, the ohmic resistance is generally higher in the case of discharge with respect to charge, except for pouch cells at the SOCs of 50% and 95%. This anomaly of pouch cells at higher SOCs may refer to an ease of extracting lithium from the anode at these states. This could indicate the formation of the SEI layer during charging at the early stages of cycling.

The 10 s instant includes both the ohmic part and the non-ohmic part of the slower dynamics or the charge transfer resistance. This non-ohmic part is attributed to the charge transfer reaction at the electrode/electrolyte interface. It also includes the mass transfer of lithium-ions. The curves for all the geometries follow the tub or upward parabolic shape, with increased resistance values at the SOC extremes. The peaks are more pronounced at the start of charging or end of discharging, i.e., at low SOC values. The flattened progression of internal resistance in the middle may be explained by more reversible kinetic and mass transport effects, with identical concentrations of products around the 50% SOC region. An interesting trend is seen around the 60-70% SOC range where the resistance curve shows a local peak for all the geometries. These local peaks are present in the case of both charge and discharge (and at the 30 s instant). It could be due to the chemical state of the reactants and products at these stages of SOC and may represent a characteristic of the 16 Ah LFP-graphite cells tested.

Comparing the resistance values among the geometries, the internal resistance of pouch is the least in most of the cases except for the end of the discharge cycle (low SOCs) where it surges ahead. For most of the cases, the internal resistance of the prismatic cell is the highest. Contrary to the expected trend, the resistance values at discharging are less than charging except for the low SOC stage. This could indicate the extraction of lithium from anode discharge is still more favorable. Although, just comparing the charge kinetic resistance in Table 5.3, it is seen that it is highest for the case of pouch cells as compared to the other geometries. This indicates the heavy influence of ohmic resistance on the 10^{th} second instant resistance.

The resistance at the 30 s instant represents the total resistance with all the ohmic and non-ohmic components. It includes the slowest dynamic or the rate-determining step and corresponds to the lithium diffusion into the active electrode material. Yet again, pouch cells show the lowest internal resistance values for all cases except at the end of the discharge cycle where its resistance is significantly higher than the other two geometries. As noticed with the 10^{th} second instant, there is a local peak on the resistance curve at around 60% SOC (for charging) and 70% SOC (for discharging), could indicate a characteristic of the 16 Ah LFP-graphite cells used. Another recurring trend is the higher value of the charge resistance as opposed to discharge resistance for mid to higher SOC values.

Comparing the diffusion polarization resistances, it is seen that pouch cell has a significantly higher resistance for the discharge pulse at 5% SOC. At the lower SOCs, the diffusion resistance seems to be high for all the geometries. On the other hand, pouch cells have the least value for the 95% SOC for both charging and discharging. Prismatic cells have a

slightly higher diffusion polarization resistance at 50% SOC than the other two packaging geometries.

Summarizing the results of the pulse test on an unaged cell, the pouch cell has the least resistance value among all the geometries, while the resistance of the prismatic cells being slightly higher than cylindrical cells in most of the cases. Though another characteristic trend is the elevated internal resistance value of pouch cell at the SOC extremities for the 10th and 30th second pulse instants, especially at the end of the discharge cycle where it rapidly surges ahead of the other two geometries. A local peak of the internal resistance of the cells tested in this work was observed around 60% SOC region for charging and 70% SOC region for discharging. The absolute values of ohmic resistance is found to be lowest for pouch cells. The ohmic component is the largest contributor to the overall resistance in most of the case, except for the discharge resistance at 5% SOC where diffusion resistances are high. The pouch cells have the highest value of charge transfer kinetic resistance.

5.2.2 Temperature developed over cycling

Data for temperature developed is processed from the first ECU of unaged cells. During the cycling, the charging was done at 1C, but the discharge was done at 0.2C, 0.5C, 1C, and 2C. Figure 5.4 shows the temperature evolved over the cycles for the three geometries, along with the voltage of the cells to represent the cycles.

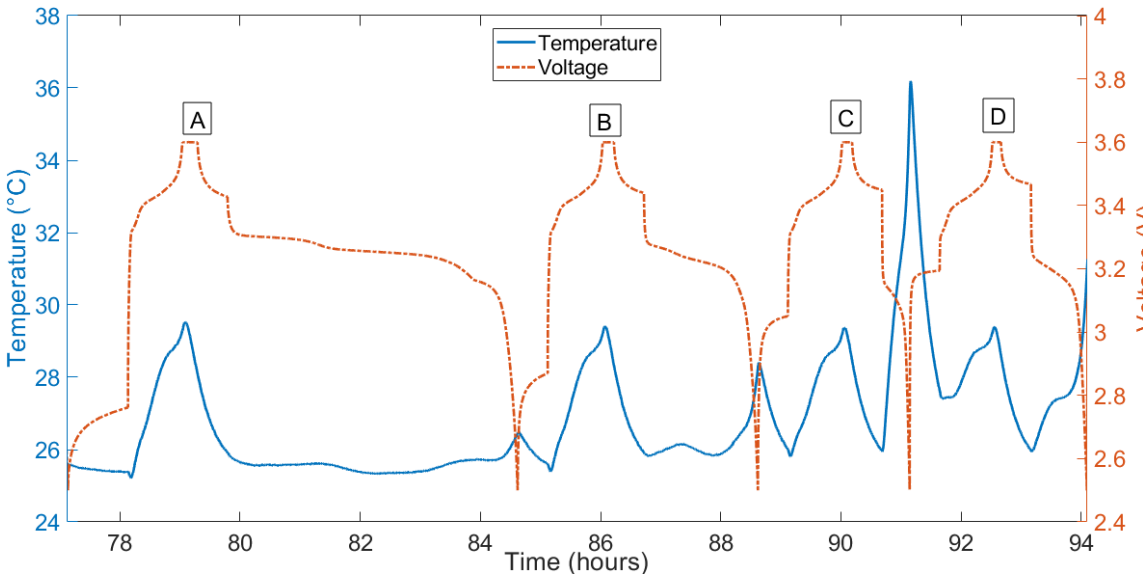

(a)

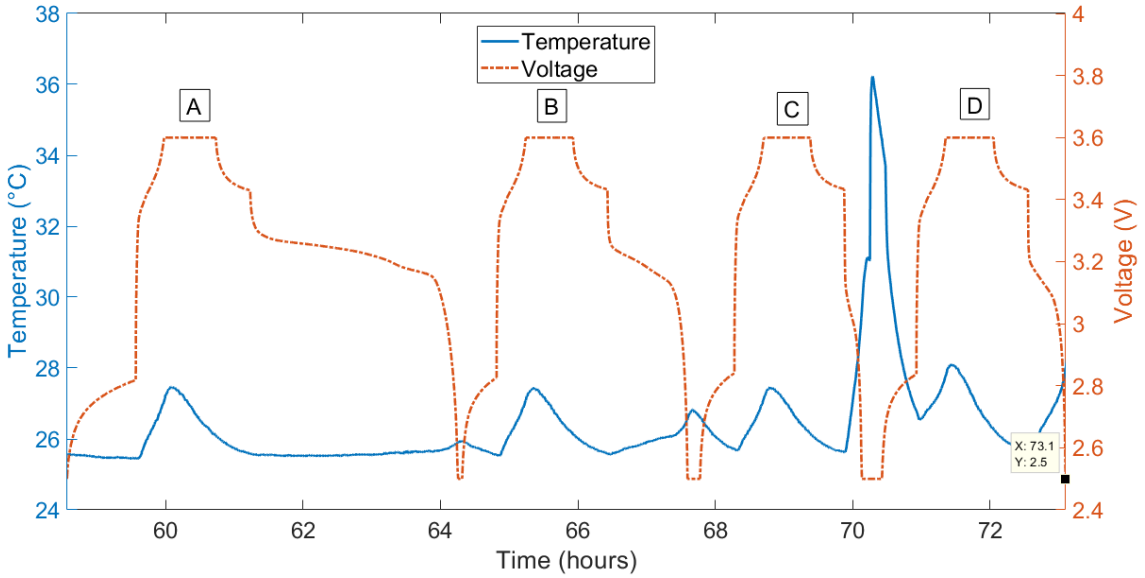

(b)

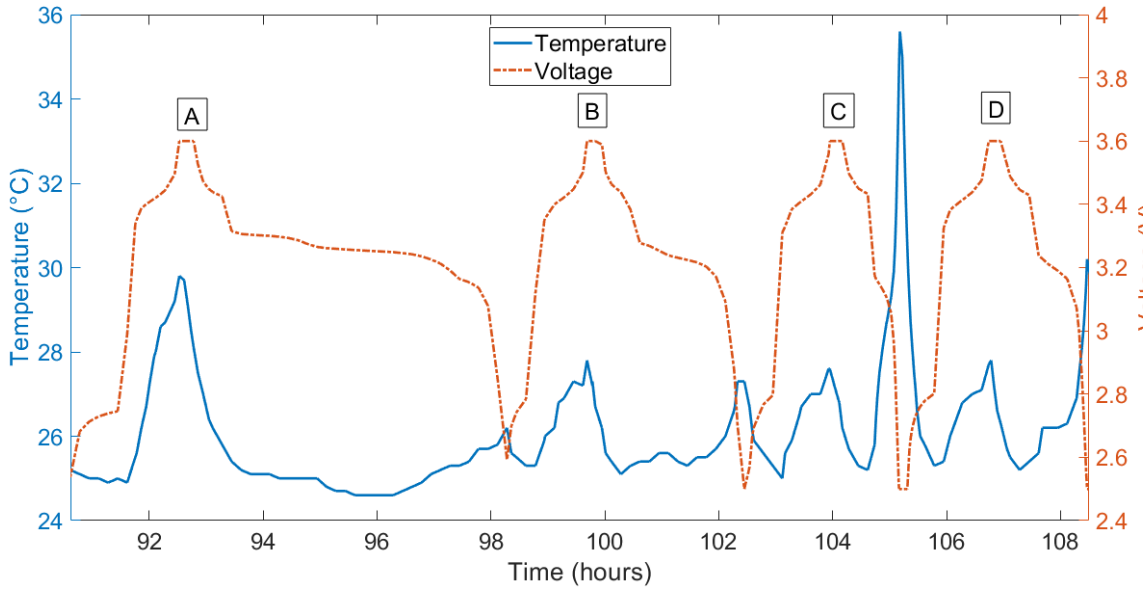

(c)

Figure 5.4. Temperature developed for (a) Cylindrical, (b) Prismatic, (c) Pouch cells

The labels in the figure refer to one cycle each and are characterized by the discharge C-rates as shown in Table 5.4.

Table 5.4. Table showing the cycle characteristic denoted by labels in Figure 5.3

Label	**A**	**B**	**C**	**D**
Charging	1C	1C	1C	1C
Discharging	0.2C	0.5C	2C	1C

The temperature profile shows a common trend among all the geometries. There are two local peaks for each cycle, one at the end of the charging cycle and one at the end of the discharging cycle. The temperature at the end of the charging cycle (at the rate of 1C) remains almost same at the end of all the charging cycles, except for the first charging cycle of pouch cell where it is slightly higher than the subsequent cycles. Table 5.5 shows the temperature gradient developed between the beginning of the charging cycle and the peak temperatures.

Table 5.5. Temperature gradient developed at different charge/discharge cycles

Cell Type	**First 1C Charge (°C)**	**1C discharge (°C)**	**2C discharge (°C)**
Cylindrical	4.14	1.83	10.19
Prismatic	2	1.34	10.51
Pouch	4.8	2.5	10.30

The first column in the table shows the temperature gradient during the charging cycle at 1C (the local peak) with respect to the temperature at the beginning of the cycle, while the next two columns show the gradient at the end of 1C and 2C discharge with respect to the temperature at the start of the cycle.

A significant observation is a global peak in temperature developed at the end of the 1C charge-2C discharge cycle for all geometries. Figure 5.5 shows a zoomed-in section for

this cycle on the same scaled axis. For each cell, the initial temperature at the start of the whole cycle, the temperature peak at the end of the first charging cycle and temperature peak at the end of the discharge cycle are also mentioned. Please note that the difference in time scale is not a significant factor as all data is for the first ECU of all geometries.

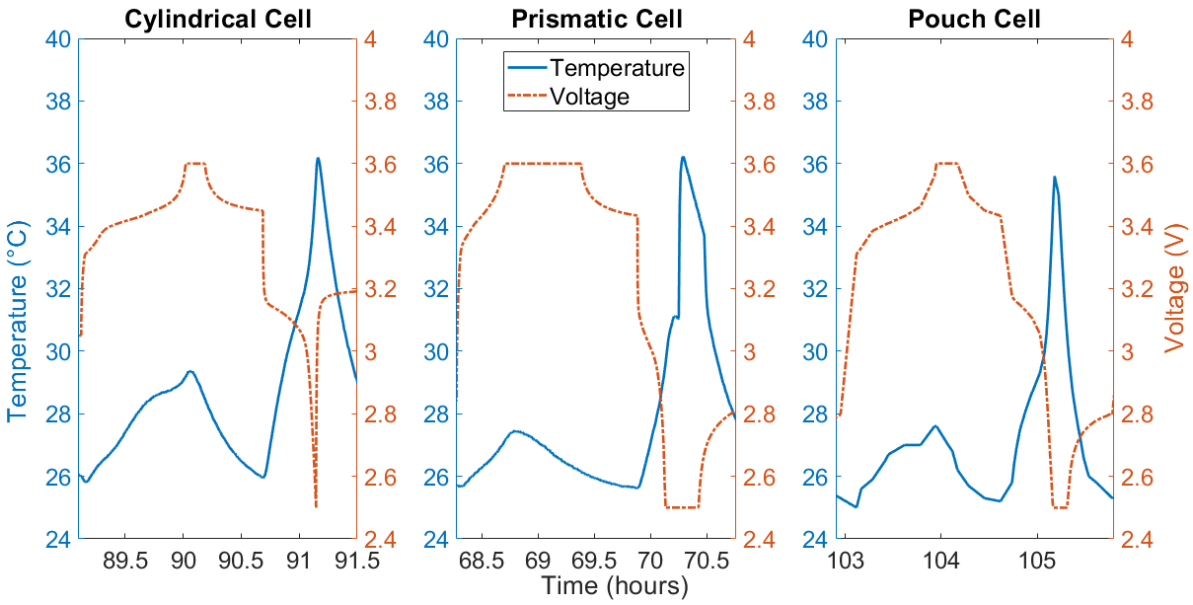

Figure 5.5. The temperature profile for 1C charge and 2C discharge for all geometries**.**

The local peak temperature at the end of the charging for the case of the cylindrical cell is higher than the other two geometries. But, the maximum temperature developed in each case remains the most important parameter for this study.

For the 1C charge-2C discharge case, while the temperature gradients are almost similar, the absolute temperature at the end of the 2C discharge is slightly lower for the pouch cell. It is corroborated by the results of the 30 s pulse test where the ohmic resistance (which leads to heating) of pouch cells is the least with prismatic cells having the highest value. This is a reasonable conclusion since the problems with thermal management and a lack of proper passage for waste heat in prismatic cells are well known [27]. This mostly because of the higher mechanical stresses. This leads to the temperatures building inside especially when subjected to rapid discharging currents. A cylindrical cell has the least surface area for heat dissipation [55], which explains the higher temperatures developed in it. As discussed earlier, pouch cells usually use thin slices of electrodes and separators which are stacked in layers. Thin electrodes can enhance the fluency of ion diffusion and improve the electrochemical reactions which helps high rate discharges and long-term performances due

to the mild temperature variation [55], which might also indicate the lower temperature developed in pouch cells and no rapid increase at 2C.

Summarizing the temperature profile results, it is observed that the peak temperatures are generated at the end of charging or at the end of discharge, while higher temperatures are reached for higher C-rates. This is because over both charge and discharge, the Li-ions migrate inside the cells to establish a concentration gradient, which generates heat as a function of applied current (Joule heating = I^2R) [56]. These temperatures are higher at the end of the discharge, which increases with an increase in discharge C-rate from 0.2C to 2C. It is expected that the temperature rise will be even higher at higher C-rates.

Better results can be expected by testing at discharge rates higher than 2C. Further, a more comprehensive study can be done with monitoring the internal temperatures developed in the cells by using embedded temperature sensors in the case of pouch cells or temperature sensors in the jelly roll structure for prismatic and cylindrical cells.

5.2.3 Summary of unaged cell tests

In this sub-section, the tests done on the unaged cells are analyzed and discussed. These are namely: 30 s pulse test for determining the internal resistance (ohmic and polarization resistances) and the temperature profile tests for different charging and discharging cycles. A correlation between the two cells are observed with the lower ohmic resistance in the case of pouch cells showing low temperature developed in them during cycling. The results are supported using literature [27] [55]. Further certain characteristics common to all the cell geometries are also established, for e.g., the internal resistance peaks at the 60-70% SOC marks both during charging and discharging, and the temperature highs at the end of charge or discharge. Based on these results, the three cell packaging geometries are compared for performance when the cells are unaged.

5.3 Aging effects on cells of different geometries

The previous section discussed the performance of the unaged cells. This section discusses the behavior of the cells during aging at the specified temperature and C-rates. The first subsection discusses the effect of aging on the 30 s pulse test results for the selected conditions of temperature and C-rates. Next, the capacity deterioration is discussed with respect to the EFC to check for aging mechanisms.

5.3.1 Change in internal resistance by aging

The 30 s pulse test, as discussed in section 5.2.1 earlier, was used on the aged cells at the cycling conditions 0.3C, 5°C and 0.3C, 45°C. The main objective was to assess the

electrochemical phenomena of the cells during the capacity fade. To achieve the same, the test data were taken from the ECUs. It must be mentioned that the different geometries tested were at different SOH at the ECUs, as shown in Table 5.6. The table also shows the number of EFCs at that SOH. It is seen from the table that cylindrical and pouch cells at 0.3C, 5°C and pouch cell at 0.3C, 45°C are past the EOL of a cell (when SOH < 80%).

Table 5.6. SOH (%) and EFC of cells for 30 s pulse test

Geometry	**SOH (%)**	**EFCs**
At 0.3C, 5°C		
Cylindrical	76.6	245
Prismatic	81.2	271
Pouch	75.4	840[9]
At 0.3C, 45°C		
Cylindrical	89.2	249
Prismatic	87.6	178
Pouch	74.5	661

The main objective is to analyze the general trends in the electrochemical behavior of the aged cells of different geometries over the whole SOC range. To best understand the data, the change in internal resistance values or internal resistance ratio (IRR) from the unaged cell values are plotted against the SOC for all the cells. The y-axis values are the ratio of the internal resistance component of aged cell to that of the unaged cells (IRR). These are plotted in Figure 5.6 and Figure 5.7. These IRRs represent the change of the specific electrochemical phenomena (ohmic and non-ohmic separated).

[9] Approximate value calculated by extrapolation

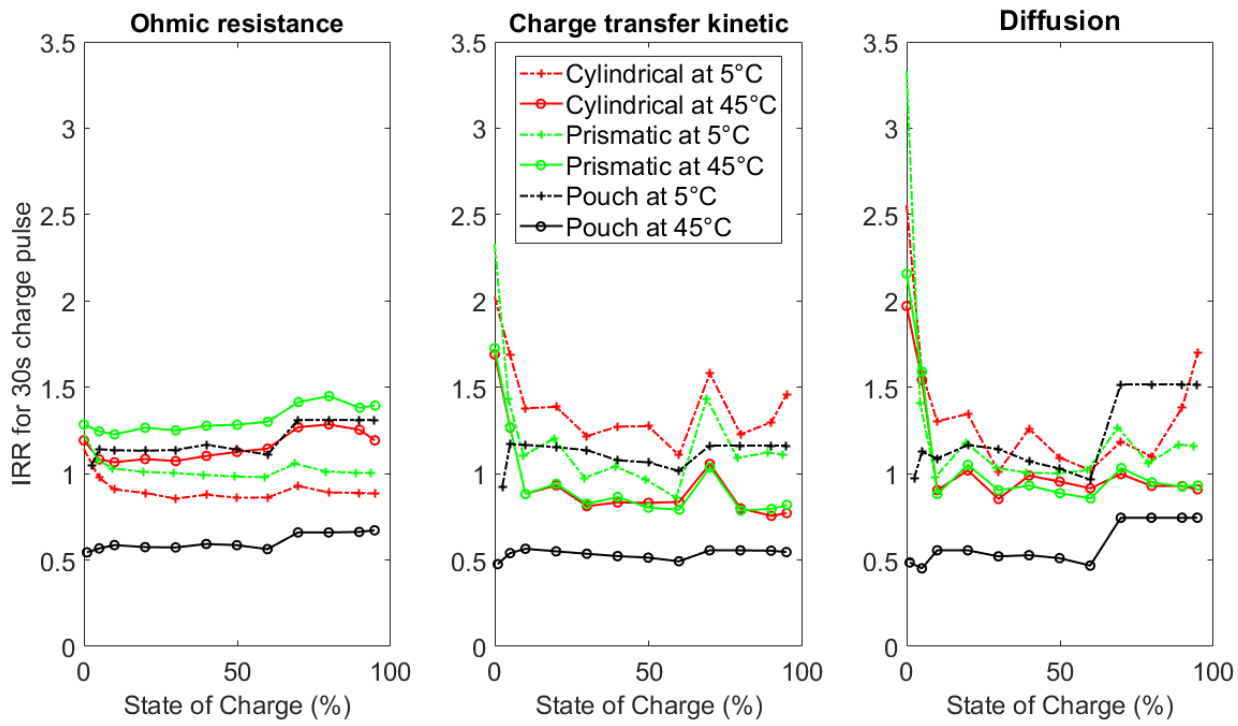

Figure 5.6. Internal resistance ratio (w.r.t. unaged cells) during 30 s charge pulse test

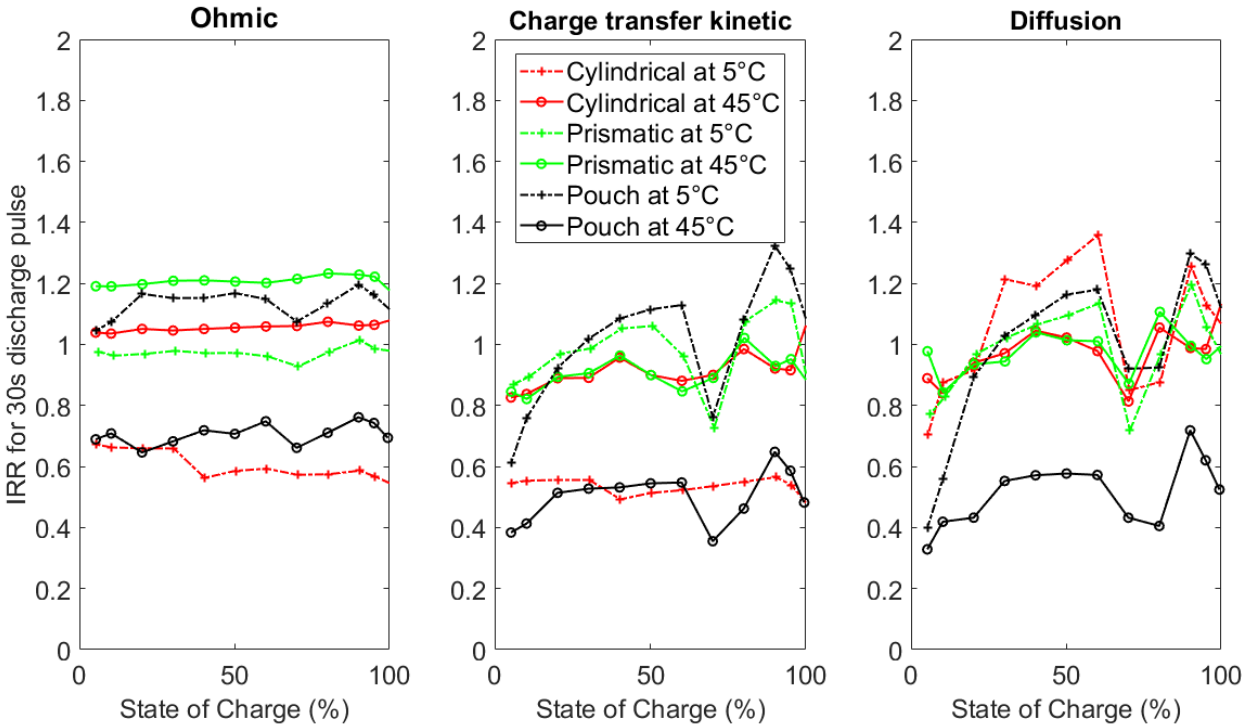

Figure 5.7. Internal resistance ratio (w.r.t. unaged cells) during 30 s discharge pulse test

Since all the cells are at different SOH stages, a direct comparison between the IRR values is unreasonable. But a comparison between the curve shapes and trends can be made.

During the charging pulse, it is noted that for low values of SOC, the IRR for charge transfer and diffusion resistance approach values as high as 3 for the prismatic and cylindrical geometries. These values then rapidly fall with further increase in SOC and then stay within a limited range. On the other hand, for pouch cells, the IRR is almost stable throughout for the ohmic and charge transfer resistances. Although, there is a rapid change around the 70% SOC mark for the case of diffusion in pouch cells. For the discharge pulse test curves, the IRRs are almost uniform and within a limited range for the ohmic resistances in all geometries. But they show rapid fluctuation in the case of the charge transfer and diffusion resistances. The range of values (minima and maxima) for each resistance component is shown in Table 5.7 and Table 5.8.

Table 5.7. Table showing minima and maxima of resistance change due to aging for a charging pulse

Charge (% change at % SOC)	**Ohmic**		**Charge transfer**		**Diffusion**	
	Minima	**Maxima**	**Minima**	**Maxima**	**Minima**	**Maxima**
For 0.3C, 5°C						
Cylindrical	14% ↓ at 30%	14% ↑ at 0%	10% ↑ at 60%	100% ↑ at 0%	1% ↑ at 30%	150% ↑ at 0%
Prismatic	2% ↓ at 60%	19% ↑ at 0%	14% ↓ at 60%	140% ↑ at 0%	0% at 50%	240% ↑ at 0%
Pouch	5% ↑ at 2.5%	31% ↑ at 70%+	8% ↓ at 2.5%	17% ↑ at 5%	3% ↓ at 2.5%	5% ↑ at 70%+
For 0.3C, 45°C						
Cylindrical	6% ↑ at 10%	28.5% ↑ at 80%	19% ↓ at 30%	69% ↑ at 0%	15% ↓ at 30%	97% ↑ at 0%
Prismatic	22% ↑ at 10%	45% ↑ at 80%	21% ↓ at 80%	72% ↑ at 0%	14% ↓ at 60%	116% ↑ at 0%
Pouch	46% ↓ at 1%	33% ↓ at 95%	53% ↓ at 1%	44% ↓ at 10%	55% ↓ at 5%	25% ↓ at 95%

Table 5.8. Table showing minima and maxima of resistance change due to aging for a discharging pulse

Discharge (% change at % SOC)	**Ohmic**		**Charge transfer**		**Diffusion**	
	Minima	**Maxima**	**Minima**	**Maxima**	**Minima**	**Maxima**
For 0.3C, 5°C						
Cylindrical	44% ↓ at 100%	33% ↓ at 5%	51% ↓ at 100%	44% ↓ at 90%	30% ↓ at 5%	35% ↑ at 60%
Prismatic	7% ↓ at 70%	1% ↑ at 90%	23% ↓ at 70%	14% ↑ at 90%	28% ↓ at 70%	20% ↑ at 90%
Pouch	5% ↑ at 5%	20% ↑ at 90%	39% ↓ at 5%	32% ↑ at 90%	60% ↓ at 5%	30% ↑ at 90%
For 0.3C, 45°C						
Cylindrical	3% ↑ at 10%	7.5% ↑ at 80%	17% ↓ at 5%	8% ↑ at 100%	19% ↓ at 70%	13% ↑ at 95%
Prismatic	16% ↑ at 100%	23% ↑ at 80%	18% ↓ at 10%	2% ↑ at 80%	16% ↓ at 10%	10% ↑ at 80%
Pouch	35% ↓ at 20%	24% ↓ at 90%	65% ↓ at 70%	35% ↓ at 90%	67% ↓ at 5%	28% ↓ at 90%

In Table 5.7 and Table 5.8, the sign ↑ refers to an increase in the resistance with respect to an unaged cell and ↓ refers to a decrease. It is interesting to note that for the pouch cell at 45°C all the resistance values have reduced from the unaged cell for both charge and discharge pulses. The cylindrical cell at 5°C also shows a consistently reduced value of ohmic and charge transfer kinetic resistances for the discharge pulse. Overall, the ohmic resistance shows lesser variations with SOC for all the geometries. Another interesting observation is that for pouch cell at 5°C, all the minima and maxima occur at 5% and 90% SOCs, respectively, for the discharge pulse. For the prismatic cell at 5°C, all the minima and maxima occur at 70% and 90% SOCs, respectively, for the discharge pulses.

For a further detailed comparison, the IRR values and the actual resistance values of the aged cells are tabulated in Table 5.9 and Table 5.10 for the SOCs 5%, 50% and 95%.

Table 5.9. Change in internal resistance due to aging (for charging pulses)

Cell type & SOH	**5%**			**50%**			**95%**		
	Ohm	***CTK***	***Dif***	***Ohm***	***CTK***	***Dif***	***Ohm***	***CTK***	***Dif***
Charging pulse for cells at 5°C/0.3C									
Cylindrical	3.11	2.57	1.75	2.87	2.15	1.75	2.82	2.62	5.20
76.6%	*0.98*	*1.69*	*1.59*	*0.86*	*1.27*	*1.09*	*0.88*	*1.46*	*1.70*
Prismatic	3.63	1.95	1.40	3.43	1.65	1.53	3.37	2.08	3.66
81.2%	*1.08*	*1.42*	*1.35*	*0.98*	*0.96*	*1.00*	*1.01*	*1.11*	*1.16*
Pouch	2.24	2.15	1.47	2.30	1.85	1.50	2.32	2.28	2.14
75.4%	*1.14*	*1.17*	*1.13*	*1.14*	*0.63*	*1.03*	*1.31*	*1.16*	*1.52*
Charging pulse for cells at 45°C/0.3C									
Cylindrical	2.88	1.79	1.46	2.82	1.51	1.48	2.66	1.54	2.35
89.2%	*1.08*	*1.27*	*1.54*	*1.13*	*0.83*	*0.95*	*1.19*	*0.77*	*0.91*
Prismatic	3.74	1.70	1.41	3.67	1.37	1.32	3.57	1.50	2.25
87.6%	*1.24*	*1.27*	*1.59*	*1.28*	*0.80*	*0.89*	*1.39*	*0.82*	*0.93*
Pouch	1.50	1.00	0.84	1.63	0.85	0.71	1.71	1.06	1.04
74.5%	*0.71*	*0.54*	*0.45*	*0.74*	*0.51*	*0.51*	*0.91*	*0.55*	*0.74*

Table 5.10. Change in internal resistance due to aging (for discharging pulses)

Cell type &SOH	**5%**			**50%**			**95%**		
	Ohm	***CTK***	***Dif***	***Ohm***	***CTK***	***Dif***	***Ohm***	***CTK***	***Dif***
Discharging pulse for cells at 5°C/0.3C									
Cylindrical	3.25	3.52	3.97	2.83	1.71	1.55	2.79	1.59	1.21
76.6%	*0.85*	*0.55*	*0.70*	*0.84*	*0.51*	*1.28*	*0.86*	*0.54*	*1.13*
Prismatic	3.73	2.99	3.49	3.42	1.32	1.27	3.36	1.30	1.08
81.2%	*0.98*	*0.87*	*0.77*	*0.97*	*1.06*	*1.10*	*0.99*	*1.13*	*1.06*
Pouch	2.15	2.57	2.35	2.01	1.52	1.35	1.97	1.55	1.22
75.4%	*1.04*	*0.61*	*0.40*	*1.17*	*1.12*	*1.16*	*1.16*	*1.25*	*1.26*
Discharging pulse for cells at 45°C/0.3C									
Cylindrical	3.03	2.61	3.27	2.75	1.24	1.23	2.70	1.16	1.04
89.2%	*1.04*	*0.83*	*0.89*	*1.05*	*0.90*	*1.02*	*1.06*	*0.92*	*0.98*
Prismatic	3.89	2.50	3.18	3.63	1.17	1.12	3.56	1.08	0.94
87.6%	*1.19*	*0.84*	*0.98*	*1.21*	*0.90*	*1.01*	*1.22*	*0.95*	*0.95*
Pouch	1.39	1.26	1.46	1.31	0.72	0.67	1.32	0.71	0.60
74.5%	*0.69*	*0.38*	*0.33*	*0.71*	*0.54*	*0.58*	*0.74*	*0.59*	*0.62*

In Table 5.9 and Table 5.10, the IRR values are mentioned in italicized numbers. The values mentioned are for the separated ohmic and non-ohmic resistances, namely: ohmic, charge transfer kinetic and diffusion polarization resistances, respectively.

It is observed from the IRRs that the internal resistances both increase and decrease for the aged cells with respect to the unaged cells. In general, the internal resistance is expected to increase with capacity deterioration. But this effect does not kick in until the latter stages of the capacity drop, which is in accordance with the studies done by Lewerenz et al. [57] and Friesen et al. [58]. According to studies done by Lewerenz et al. [57], the internal resistance

is either constant or decreasing during the cycling, and it increases rapidly only when the capacity becomes very low or cut-off voltages are reached during cycling. The start of the rapid increase in internal resistance depends on whether the aging conditions are severe (internal resistance increase at around 80-85%) or mild (internal resistance increase at around 70%) [57].

Rapid capacity fade due to the aging phenomena also lead to an early onset of rapid internal resistance increase. Friesen et al. [58] have plotted internal resistance evolution curves over the number of EFCs and the curves have the upward parabolic shape. The internal resistance of the cells studied by them decrease until about the first 100-150 EFCs, after which they rise and only reach values equal to an unaged cell after around 300-320 EFCs for low-temperature cells and about 800 EFCs for high-temperature cells [58]. This initial decrease in internal resistance is attributed to the formation of a more effective SEI with a lower lithium-ion migration and charge transfer resistances [58]. These studies explain the internal resistance ratios less than 1 shown in Figure 5.6 and Figure 5.7.

The 0.5th second or the ohmic component of the internal resistance is also seen to both increase and decrease with aging for all the geometries. As mentioned in Table 3.1 in section 3.2.2, the ohmic resistance consists of different components: ionic, electrical and interfacial. The changes in the ohmic resistance on aging are governed by these components. For example, the electrolyte resistance depends on its conductivity, which changes with the concentration of conductive salt dissolved in it [59]. The deterioration of the ionic, electrical and interfacial factors may lead to increase in the ohmic resistance. But the literature studied did not include any reason for reduction of ohmic resistance for the aged cells[10].

For the cylindrical cells, the resistances at 45°C are seen to be lower than at 5°C. Though this could be because the cell at 45°C as at a much higher SOH stage (89.2%) than the cell at 5°C (76.6%). For both the cells (at 5°C and 45°C), the resistance values increase from charge to discharge for the SOCs 5% and 50%. While the opposite trend is true for the 95% SOC. This resembles the trend already seen for unaged cells in section 5.2.1. The ohmic resistance undergoes the least changes with respect to SOC. Overall, the values of the

[10] This could be because of the approximation to consider the 0.5th second resistance as the ohmic resistance. In ideal cases, by the 0.5th second, the charge transfer kinetics have also kicked in. Further studies are required to verify this inference.

resistances are almost similar, with the ohmic resistances marginally higher than the other resistances. The exceptions are the discharge pulse resistances at 5% SOC where the diffusion resistance is higher. Further, the diffusion resistance for the cylindrical cell at 5°C is significantly high (5.201 mOhm) at 95% SOC for the charging pulse.

The resistance comparison of the prismatic cells at 5°C (SOH 81.2%) and 45°C (SOH 87.6%) do not reveal any trend. For both kinds of cells, the cell resistances either remain almost the same or increase from discharge pulse to charge pulse for the SOCs 50% and 95%. Whereas, in the case of the SOC 5%, the resistance increases from charge pulse to discharge pulse. This again resembles the trend for unaged prismatic cells studied in section 5.2.1. The ohmic resistances also remain almost similar for both kinds of pulses. Overall the ohmic resistance is usually higher than the other two components. The exception is the diffusion resistance at 95% SOC for the cell at 5°C.

The pouch cells tested at 5°C and 45°C are both at similar SOHs, 75.4% and 74.5% respectively. Therefore, a comparison between the resistances of these two types of cells is more reliable. It is seen that the resistances of the cell at 5°C is higher than the one at 45°C. This could indicate a worse performance of pouch cells at low temperatures. Comparing the charge and discharge resistances, the resistance increases from discharge to charge for the 50% and 95% SOCs. Whereas, the charge transfer and diffusion resistances decrease from discharge to charge. This almost resembles the trend observed for the unaged pouch cell in section 5.2.1, except for the case of the ohmic resistances. The ohmic resistance always increases from discharge to charge. Further, the ohmic resistance change between the charge and discharge pulse is rather significant when compared with the other two geometries. Ohmic resistance remains higher than the other two components for the 50% and 95% SOCs. Whereas, the diffusion and ohmic resistances are identical for the 5% SOC.

Comparing the three geometries, pouch cells show the least resistances despite having reached lower SOH values. Combined with the EFC values from Table 5.6, it also indicates that the pouch cells can retain lower internal resistances for more equivalent cycles than the cylindrical and prismatic cells. Further, for all the geometries, the most significantly increased component of the resistance could indicate the phenomena most affected by aging. This is shown in Table 5.11. This summarizes the information given in Table 5.7 and Table 5.8. It is interesting to note that for both kinds of cylindrical cells, the electrochemical phenomena related to diffusion is most affected by aging. The same is true for prismatic cells as well. The exception for the case of prismatic cells for the discharge pulse in the 45°C cell where the ohmic resistance has increased the most. For the pouch cells at higher temperature, the resistance is still lower than for the unaged cells at the time of testing, therefore, it is not possible to infer which resistance component is increasing the most.

Table 5.11. Dominant resistance increase factor at different SOC values

Pulse	**Cylindrical**	**Prismatic**	**Pouch**
For cells at 5°C/0.3C			
Charge	Diffusion	Diffusion	Ohmic
Discharge	Diffusion	Diffusion	Charge transfer
For cells at 45°C/0.3C			
Charge	Diffusion	Diffusion	-
Discharge	Diffusion	Ohmic	-

Summarizing the results from this section, it was first proved via literature [57] [58], that the cell resistance does not increase for a rapidly for a first few cycles and may even decrease. The resistance rapidly increases only around the EOL of the cell or after the cut-off voltage has been reached. Further, the general trends of the curves of the incremental change of resistance over SOC are compared for the different cell geometries. In pouch cells, the high number of EFCs and low internal resistances indicated a reliable performance of the cell over many cycles. Comparing the IRR curves over SOC, it is seen that the IRR in the case of ohmic resistance is more stable than the other two components of resistance. Charge transfer and diffusion resistances show significant higher values at the start of the charge pulse in the case of prismatic and cylindrical cells. For both the cylindrical and prismatic cells, the ohmic resistance variation is minimal from charge to discharge pulse. For pouch cells, on the other hand, the ohmic resistances vary significantly from charge to discharge pulses. It is also seen that the resistances value for pouch cell at 45°C are lower than that of 5°C, hinting at reduced performance of pouch cells at lower temperatures. Further, the pouch cells are found to retain lower resistance values for a higher number of EFCs as compared to cylindrical and prismatic cells. Further, it was found that the diffusion related electrochemical phenomena are affected the most by aging for the cylindrical and prismatic cells.

5.3.2 Aging characteristics over the equivalent full cycle

The previous chapter discussed the effect of aging on the internal resistance and electrochemical phenomena within the cells. In this section, the capacity fade over EFCs is discussed for cells at different conditions. The concept of EFC has already been discussed in Chapter 4. The capacity undergoes changes because of the cyclic and storage deterioration. Different cell chemistries, therefore, show a different drop in capacities. At the same time, the number of EFCs possible within the lifetime of the cell (drop to 80% SOH) also differ from one cell to another. Figure 5.8 shows the EFCs for each geometry of cell for different cell conditions over the aging period as shown by the SOH. As discussed already, the SOH has been determined by a drop of the capacity of the cells, therefore SOH is used as the parameter to describe the aging process.

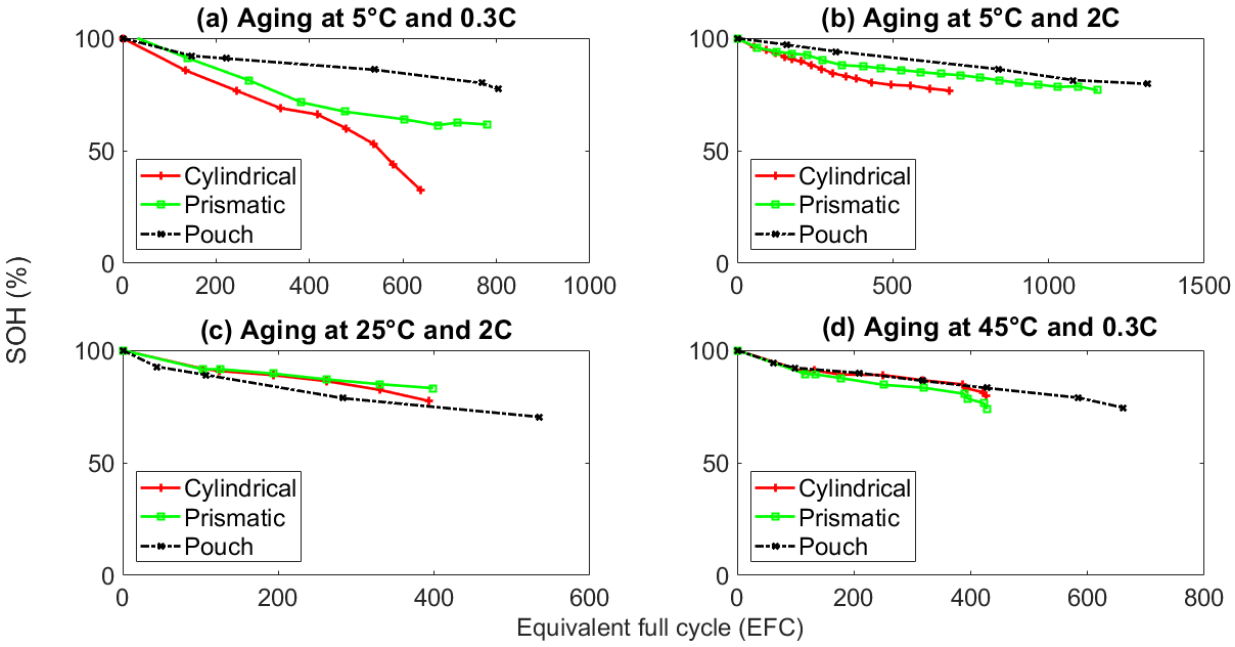

Figure 5.8. Capacity deterioration and the number of equivalent cycles obtained over the aging period for the cycling conditions (a) 5°C, 0.3C; (b) 5°C, 2C; (c) 25°C, 2C; (d) 45°C, 0.3C

The effect of the charge-discharge protocols is uniform for all the cells. Another major influencing factor on the capacity fade is the DOD, but it has not been considered here as all the cells are cycled between 0% and 100% SOC.

The importance of SEI layer and its properties in an ideal condition has been discussed in Chapter 3. In real cases, the SEI layer thickens by repeated cycling gradually due to electron exposure to electrolyte and electrolyte diffusion to the graphite surface. This not only leads to electrolyte decomposition but also might lead to loss of active lithium [40]. The four different aging mechanisms attempt to explain the various ways in which this can happen.

Therefore, this study primarily analyses the aging phenomenon with respect to the SEI layer formation and the related four aging mechanisms [31]. It must also be noted that most studies agree to deal with the cycle number as the main time notion, and therefore, the aging curves here are plotted against the EFC. While in practice higher C-rates should accelerate the aging of the cells, but in practice, the relation between C-rates and the capacity fade is found to be complex [31] [32]. Even so, the highest C-rate in this study (2C) does not have a significant effect on the aging mechanism. Aging and SEI layer formation strongly depend on the cycling temperature. There is an optimum temperature (usually moderate temperatures) for cycling which may be different for each cell. Temperatures above this favor further SEI layer formation and thus accelerate aging [60].

The aging curves in Figure 5.8 show a low capacity degradation in the case of pouch cells as compared to other geometries in all but one operating condition (25°C, 2C). For a thorough analysis, the capacity after 400 EFCs are tabulated all the geometries under all operating conditions. It is shown in Table 5.12.

Table 5.12. Table showing the remaining capacities of cells, in terms of SOH, after 400 EFCs

Cycling conditions	**Remaining capacity in terms of SOH after 400 EFCs (%)**		
	Cylindrical	**Prismatic**	**Pouch**
5°C, 0.3C	66.69	70.70	88.13
5°C, 2C	81.40	87.49	92.84
25°C, 2C	76.94	83.12	74.82
45°C, 0.3C	82.63	78.10	84.02

In cylindrical cells, the capacity fade at 5°C and 0.3C is the lowest. But any increase in either the C-rate or the temperature leads to a slower capacity fade. This directly indicates the influence of the aging mechanism related to Lithium plating. Low temperatures affect the anode kinetics and result in the reduction of the solid state ionic diffusion rate, which increases the risk of lithium plating. At higher C-rates or temperatures, the anode kinetics improve and thus resulting in reduced cell degradation rate, with higher temperatures being more suitable for maintaining a higher capacity [30]. Further the higher degradation rate for the case of the cell at 25°C, 2C is attributed to the combined effect of higher temperature developed due to the cycling temperature and higher cycling rate (it was observed in a

previous section that temperature developed in cylindrical cells at 2C charge rate is the highest). Higher temperatures developed due to the combined factors can damage the morphology of the SEI layer leading to decomposition of the electrolyte. A further aging mechanism can be particularly seen in the case of the cylindrical cell at 5°C and 0.3C, which is the LAM, characterized by the abrupt capacity losses during the latter stages of aging, which indicates structural degradation of electrodes at this stage [30]. Minor evidence of LAM is also seen at the end of the curve at 45°C and 0.3C.

For the case of prismatic cells, the trend resembles cylindrical cells, but with a lower rate of capacity deterioration. This might be because of lithium plating but at a lower degree. Further, no evidence of hidden capacity loss due to LAM is seen in this case, except for a minor evidence of it at 45°C and 0.3C resembling the cylindrical cells at the same condition. This follows expectations as LAM is higher at elevated temperatures.

The pouch cells have the best capacity retention out of all the geometries under most cycling conditions (except one anomalous condition of 25°C and 2C). Since all the graphite anode based lithium-ion cells show initial aging due to the formation of SEI layers on the electrode, it can be inferred that the SEI layer in the case of pouch cells not only has the minimum surface area but is also the most uniform and most stable [30] [31] [40]. This might be because of the less mechanical and thermal stresses in the geometry of pouch cells due to the stacked structure and soft casing. This can potentially be a significant advantage of pouch cells compared to cylindrical and prismatic geometries, with respect to SEI layer formation. This is inferred because the only factor determining the ideal SEI layer not common to all the geometries is the tolerance to expansion and contraction stresses (mechanical stresses).

The pouch cells also undergo improved capacity retention moving from 5°C, 0.3C to 5°C, 2C, resembling both cylindrical and prismatic geometries, suggesting a small lithium plating induced LLI process because of reduced kinetics at low temperatures and low C-rate. Overall, pouch cells show a much better performance at lower temperatures. But the effect of high temperature induced SEI layer formation (temperature increase from 5°C to 45°C) overcompensates any improvement in the kinetics and results in faster capacity fade at higher temperatures. It must be noted that the behavior of pouch cells at 25°C and 2C is anomalous and cannot be explained suitably with the literature studied.

Summarizing the results, it is observed that the pouch cells have the best overall capacity retention among all structures and is particularly favorable towards the formation of an ideal SEI layer. Further, it is observed that all the geometries undergo lithium plating at low temperatures of operation. A comparison of the high-temperature capacity fading suggests that

the optimum temperature of cycling is highest for cylindrical cells followed by prismatic cells with pouch cells having the least. Both the prismatic and cylindrical geometries show tendencies of LAM with an abruptly increased capacity fade, with the cylindrical cell at 5°C and 0.3C showing a significant drop. Any instances of LAM could also suggest a possible electrode deterioration.

After the capacity deterioration studies, the cells from two different conditions of cycling (namely, 0.3C, 5°C and 0.3C, 45°C) were chosen for 30 s pulse tests to determine the effect of capacity fade on the internal resistance and the polarization in the cells.

5.3.3 Summary of tests on aged cells

In this subsection, first, the capacity deterioration of aged cells was studied for different conditions of operating temperatures and C-rates. The different capacity fade mechanisms were analyzed. Cylindrical cells, especially, and to some extent, prismatic cells showed evidence of lithium plating at low temperatures. The performance of pouch cells was better at low temperatures. Cylindrical cells show the highest operating temperatures while the pouch cells have the least. Overall, the capacity retention of pouch cells is the best among all geometries.

Further, 30 s pulse tests were performed on cells with the same C-rate (0.3C) and two different temperatures (5°C and 45°C). A direct comparison between the cells as all of them is at different SOHs during the check-ups (ECU). The tests gave information about the electrochemical phenomena. Many resistance and polarization values seemed to reduce with respect to the unaged cell. This was validated using previous studies and it was inferred that the actual resistance increase kicks off around the EOL of the cells or on reaching the cut-off voltage and depends on the severity of cycling conditions. It was seen that the elevated increase in diffusion polarization concurs with the lithium plating occurring for cylindrical cells at low temperatures. Prismatic cells show an elevated ohmic resistance increase at higher SOCs while discharging. The aged pouch cells show the highest fluctuations in resistance and polarization values with respect to the unaged cells. It is also evident that the capacity deterioration and rapid internal resistance increase for pouch cells kicks in at a much lower SOH and can undergo higher number of EFCs

6 Summary

The objective of the thesis was to analyze the performance of 16 Ah LFP-graphite cells with respect to their packaging geometries. The literature studied indicated limited studies on performance comparison of lithium-ion cells based on packaging geometries. The initial chapters discussed the fundamentals of lithium-ion cells with a focus on the $LiFePO_4$ cells. The different packaging geometries were introduced and studied based on their structures with illustrations and examples of applications.

The literature reviewed discussed the state of the art in the study of comparison of lithium-ion cell packaging geometries. The aging mechanisms were studied with a focus on the importance of SEI layer formation and its contribution in capacity deterioration. The aging of the cell shows changes in the internal resistance which directly affects properties like capacity, power density, energy density etc. The different types of internal resistances were discussed. Different methods to measure and separate resistance based on electrochemical stages were studied focusing more on DC pulse methods to measure resistances. It was found that the DC pulse method is not completely capable of separating the resistances according to the electrochemical phenomena, but a suitable approximation was used for the further tests and analyses.

The cylindrical and prismatic were prepared using jelly roll manufacturing, while the pouch cells, on the other hand, were manufactured by zig-zag thin layers of electrodes and separators. Reception tests showed higher energy density of the pouch cells which can be attributed to the light aluminum pouch cover. Further, the zig-zag layering of thin slices of electrodes and separators is shown to have the highest packing density, thus reducing the packing material required.

The unaged cells were first tested for a performance analysis. Only cyclic aging tests were considered in the whole scope of the thesis. The pouch cells showed the lowest internal resistance, which was attributed to the thinner electrodes and less distance for ion diffusion. It must be noted that the lithium-ion diffusion in the active electrode material is the rate determining step. The pouch cells have the least resistance value among all the geometries, while the resistance of the prismatic cells having the highest. The anomaly with pouch cell is the elevated resistance at the SOC extremities for the 10^{th} and 30^{th} second pulse instants, especially at the end of the discharge cycle. The absolute values of ohmic resistance is

found to be lowest for pouch cells. The ohmic component is the largest contributor to the overall resistance in most of the case, except for the discharge resistance at 5% SOC where diffusion resistances are high. The pouch cells have the highest value of charge transfer kinetic resistance. The temperature evolution in the cells followed from the ohmic resistance of the cells with pouch cells getting the least warm and prismatic cells getting the hottest. The peaks in temperatures were at the end of the charge and discharge cycles, with higher current rate during discharge leading to higher temperatures.

The cells were further analyzed to check the effect of aging on electrochemical activity. It was proved that initially the internal resistance remains almost constant or even goes down before the severity of the cycling conditions determines when the actual rapid rise of internal resistance starts (typically around the EOL mark). The pouch cells showed evidence of a very late onset of a rapid internal resistance increase. It was found that the diffusion related electrochemical phenomena are affected the most due to aging for the case of cylindrical and prismatic cells. The effect of aging on the capacity deterioration was studied next. Cylindrical and prismatic cells showed evidence of lithium plating at lower temperatures. They also showed the characteristic sudden decrease in capacity at higher EFCs which is associated with the loss of active material (LAM) due to electrode deterioration. The pouch cells have the best capacity retention over many cycles. One of the reasons for it is attributed to the uniform and stable SEI layer formed due to the less mechanical and thermal stresses in the geometry of pouch cells due to the stacked structure and soft casing. A comparison of the cycling temperatures of the cells shows that the cylindrical cells have the highest optimum temperature while pouch cells have the least.

7 Prospect

The rising significance of sustainability in mobility and renewable energy storage systems has necessitated the further research into cheaper and safer Lithium-ion batteries. LFP-graphite cells have become popular as safer options. But further research is required to make the technology cheaper and its application more widespread. The study of different packaging geometries opens a totally new area of research to explore the technology further. For instance, it could open more possibilities where certain applications are more suited to certain geometries. As studied in this thesis, the comparison study of cells of similar chemistry and design capacity but with different geometries is still at a very pristine stage. This thesis is a first such study of the performance analysis of these packaging geometries, which elevates the scope of this work.

The scope of this thesis can be further increased by improving on the tests performed. For instance, to get a better approximation of the temperature developed within the cell, embedded temperature sensors in the case of pouch cells or temperature sensors in the jelly roll structure of the prismatic and cylindrical cells can be used as used in some past studies. Further, the temperatures can be calculated for charging pulses at more than 1C current rate as done in this study. Temperature rise at higher C-rates, especially above 5C have shown much higher temperature rise and gives much better values for a thorough comparison. Similarly, more conditions of cycling temperature and C-rates would help in more thorough knowledge about their effects in the different geometries. The DC pulse tests on the aged cells were done on cells of different SOHs which does not make it possible to perform a direct comparison between the geometries. Ideally, the ECUs can be performed on set values of mid-of-life (MOL) and EOL. A post mortem studies of these cells can also be interesting. Moreover, the DC pulse test fails to exactly separately the resistances and polarizations, and other methods like AC tests or EIS can be performed. Further, calendar aging tests can give some interesting insights into the behavior of the packaging geometries.

The purpose of this study is to pave way for further studies in this field of research. In the future, these tests can be adapted to more specific applications, for e.g., using data from testing stage electric vehicles.

Bibliography

[1] Buchmann, Isidor. BU-1003: Electric Vehicle (EV). Battery University, Cadex Electronics Inc (2018).

[2] Grandjean, Thomas; Barai, Anup; Hosseinzadeh, Elham; Guo, Yue; McGordon, Andrew; Marco, James. Large format lithium ion pouch cell full thermal characterisation for improved electric vehicle thermal management. Journal of Power Sources. 359 (2017).

[3] Erriquez, Mauro; Morel, Thomas; Schäfer, Philip; Moulière, Pierre-Yves. Trends in electric-vehicle design. McKinsey&Company, Automotive & Assembly (October 2017).

[4] Alarco, Jose; Talbot, Peter. The history and development of batteries (2015).

[5] Blomgren, George E. The Development and Future of Lithium Ion Batteries. Journal of The Electrochemical Society. 164 (2016).

[6] Nitta, Naoki; Wu, Feixiang; Lee, Jung Tae; Yushin, Gleb. Li-ion battery materials. Materials Today. 18 (2015).

[7] Saha, Bhaskar; Goebel, Kai. Modeling Li-ion battery capacity depletion in a particle filtering framework (2009).

[8] Battery Universe. Difference Between Nicad NiMH and Li-Ion Battery Cells. Battery Universe.

[9] Galushkin, N. E.; Yazvinskaya, N. N.; Galushkin, D. N. Mechanism of Thermal Runaway in Lithium-Ion Cells. Journal of The Electrochemical Society. 165 (2018).

[10] Soylu, Seref. Electric Vehicles - The Benefits and Barriers (2011). 978-953-307-287-6.

[11] Buchmann, Isidor. BU-205: Types of Lithium-ion. Battery University, Cadex Electronics Inc (2018).

[12] Padhi, A. K. Phospho-olivines as Positive-Electrode Materials for Rechargeable Lithium Batteries. Journal of The Electrochemical Society. 144 (1997).

[13] Eftekhari, Ali. LiFePO 4 /C nanocomposites for lithium-ion batteries. Journal of Power Sources. 343 (2017).

[14] Athena Combs-Hurtado; Marc Hensel. Memorandum: Using Lithium Iron Phosphate Batteries for Utility Scale Storage Applications. Arizona State University (21 October 2017).

[15] Zhang, Xiangwu; Ji, Liwen; Toprakci, Ozan; Liang, Yinzheng; Alcoutlabi, Mataz. Electrospun Nanofiber-Based Anodes, Cathodes, and Separators for Advanced Lithium-Ion Batteries. Polymer Reviews. 51 (2011).

[16] Jow, T. Richard; Delp, Samuel A.; Allen, Jan L.; Jones, John-Paul; Smart, Marshall C. Factors Limiting Li + Charge Transfer Kinetics in Li-Ion Batteries. Journal of The Electrochemical Society. 165 (2018).

[17] Jow, T. R.; Allen, Jan L.; Deveney, Bridget; Nechev, Kamen. Charge Transfer and Charge-Discharge Kinetics in Lithium-ion Batteries (October 12 - October 17, 2008).

[18] Valoen, Lars Ole; Reimers, Jan N. Transport Properties of LiPF[sub 6]-Based Li-Ion Battery Electrolytes. Journal of The Electrochemical Society. 152 (2005).

[19] Lundgren, Henrik. Thermal aspects and electrolyte mass transport in lithium-ion batteries. TRITA-CHE-Report. 2015:22 (2015). 978-91-7595-584-1.

[20] Gao, Jian; Shi, Si-Qi; Li, Hong. Brief overview of electrochemical potential in lithium ion batteries. Chinese Physics B. 25 (2015).

[21] Buchmann, Isidor. BU-301a: Types of Battery Cells. Battery University, Cadex Electronics Inc (2018).

[22] Schröder, Robert; Aydemir, Muhammed; Seliger, Günther. Comparatively Assessing different Shapes of Lithium-ion Battery Cells. Procedia Manufacturing. 8 (2017).

[23] Jessica Shankleman; Tom Biesheuvel; Joe Ryan; Dave Merrill. We’re Going to Need More Lithium. Bloomberg LP (2017).

[24] AUDI Digital Illustrated. AUDI future performance 2015 illustrated. AUDI Illustrated (2016).

[25] Jaggi, Anmol. Comparison of different Li-ion cell types. Gensol Engineering Pvt. Ltd. (Jan 26, 2017).

[26] Ahn, Soonho; Lee, Hyang-Mok; Lee, Seung-Jin; Youngsun, Park; Ku, Cha-Hun; Kim, Je Young; Lee, Jae-Hyun; Kim, Seok Koo; Cho, Jin Yeon. The Impact of Cell Geometries and Battery Designs on Safety and Performance of Lithium Ion Polymer Batteries. Batteries R&D, LG Chemical Ltd./ Research Park.

[27] Maiser, Eric. Battery packaging - Technology review (2014).

[28] Mulder, Grietus; Omar, Noshin; Pauwels, Stijn; Meeus, Marcel; Leemans, Filip; Verbrugge, Bavo; Nijs, Wouter de; van den Bossche, Peter; Six, Daan; van Mierlo, Joeri. Comparison of commercial battery cells in relation to material properties. Electrochimica Acta. 87 (2013).

[29] Zhao, Jingyuan. Cycle life testing of lithium batteries. International Journal of Electrochemical Science (2018).

[30] Anseán González, David. High power li-Ion battery performance: a mechanistic analysis of aging (2015).

[31] Barré, Anthony; Deguilhem, Benjamin; Grolleau, Sébastien; Gérard, Mathias; Suard, Frédéric; Riu, Delphine. A review on lithium-ion battery ageing mechanisms and estimations for automotive applications. Journal of Power Sources. 241 (2013).

[32] Sarasketa-Zabala, E.; Gandiaga, I.; Martinez-Laserna, E.; Rodriguez-Martinez, L. M.; Villarreal, I. Cycle ageing analysis of a LiFePO4/graphite cell with dynamic model validations. Journal of Power Sources. 275 (2015).

[33] Pinson, M. B.; Bazant, M. Z. Theory of SEI Formation in Rechargeable Batteries. Journal of the Electrochemical Society. 160 (2012).

[34] Han, Xuebing; Ouyang, Minggao; Lu, Languang; Li, Jianqiu; Zheng, Yuejiu; Li, Zhe. A comparative study of commercial lithium ion battery cycle life in electrical vehicle. Journal of Power Sources. 251 (2014).

[35] Sun, Shun; Guan, Ting; Shen, Bin; Leng, Kunyue; Gao, Yunzhi; Cheng, Xinqun; Yin, Geping. Changes of Degradation Mechanisms of LiFePO4/Graphite Batteries Cycled at Different Ambient Temperatures. Electrochimica Acta. 237 (2017).

[36] Lewerenz, Meinert; Marongiu, Andrea; Warnecke, Alexander; Sauer, Dirk Uwe. Differential voltage analysis as a tool for analyzing inhomogeneous aging. Journal of Power Sources. 368 (2017).

[37] Uddin, Kotub; Perera, Surak; Widanage, W.; Somerville, Limhi; Marco, James. Characterising Lithium-Ion Battery Degradation through the Identification and Tracking of Electrochemical Battery Model Parameters. Batteries. 2 (2016).

[38] Frank Kindermann. The Solid-Electrolyte Interface (2012).

[39] Xu, Kang. Nonaqueous Liquid Electrolytes for Lithium-Based Rechargeable Batteries. Chemical Reviews. 104 (2004).

[40] An, Seong Jin; Li, Jianlin; Daniel, Claus; Mohanty, Debasish; Nagpure, Shrikant; Wood, David L. The state of understanding of the lithium-ion-battery

graphite solid electrolyte interphase (SEI) and its relationship to formation cycling. Carbon. 105 (2016).

[41] Zhou, Daming; Zhang, Ke; Ravey, Alexandre; Gao, Fei; Miraoui, Abdellatif. Parameter Sensitivity Analysis for Fractional-Order Modeling of Lithium-Ion Batteries. Energies. 9 (2016).

[42] Barai, Anup; Uddin, Kotub; Widanage, W. D.; McGordon, Andrew; Jennings, Paul. A study of the influence of measurement timescale on internal resistance characterisation methodologies for lithium-ion cells. Scientific reports. 8 (2018).

[43] Park, Myounggu; Zhang, Xiangchun; Chung, Myoungdo; Less, Gregory B.; Sastry, Ann Marie. A review of conduction phenomena in Li-ion batteries. Journal of Power Sources. 195 (2010).

[44] Raghavendra Arunachala. Influence of Cell Size on Performance and Lifetime of Lithium-Ion Batteries. Technische Universität München (November 16, 2017).

[45] Vetter, J.; Novák, P.; Wagner, M. R.; Veit, C.; Möller, K.-C.; Besenhard, J. O.; Winter, M.; Wohlfahrt-Mehrens, M.; Vogler, C.; Hammouche, A. Ageing mechanisms in lithium-ion batteries. Journal of Power Sources. 147 (2005).

[46] Palcoux, G.; Schmalz, J.; Richter, L.; Porcher, W. SPICY Deliverable D5.6. CEA, TUM-PROLLION (30 June 2015).

[47] Yaakov, David; Gofer, Yossi; Aurbach, Doron; Halalay, Ion C. On the Study of Electrolyte Solutions for Li-Ion Batteries That Can Work Over a Wide Temperature Range. Journal of The Electrochemical Society. 157 (2010).

[48] Trad, Khiem; Mulder, Grietus; Gutiérrez, César; Meatza, Iratxe de; Delaille, Arnaud; Porcher, Willy. SPICY Deliverable D6.1. CIDETEC, CEA, TUM, PROLLION (21 August 2015).

[49] M. Nisvo Ramadan; Bhisma A. Pramana; Adha Cahyadi; Oyas Wahyunggoro. State of health estimation in lithium polymer battery (2016).

[50] Li, Lian-xing; Tang, Xin-cun; Qu, Yi; Liu, Hong-tao. CC-CV charge protocol based on spherical diffusion model. Journal of Central South University of Technology. 18 (2011).

[51] Svens, Pontus; Behm, Mårten; Lindbergh, Göran. Lithium-Ion Battery Cell Cycling and Usage Analysis in a Heavy-Duty Truck Field Study. Energies. 8 (2015).

[52] Liu, Guang; Guo, Liang; Liu, Chunlong; Wu, Qingwen. Evaluation of different calibration equations for NTC thermistor applied to high-precision temperature measurement. Measurement. 120 (2018).

[53] Chang, Wen-Yeau. The State of Charge Estimating Methods for Battery. ISRN Applied Mathematics. 2013 (2013).

[54] Liu, Chaofeng; Neale, Zachary G.; Cao, Guozhong. Understanding electrochemical potentials of cathode materials in rechargeable batteries. Materials Today. 19 (2016).

[55] Zhao, Rui; Zhang, Sijie; Gu, Junjie; Liu, Jie. 2016 IEEE Electrical Power and Energy Conference (EPEC). IEEE Electrical Power and Energy Conference; Annual IEEE Electrical Power and Energy Conference; Conférence sur l'énergie électrique de l'IEEE; EPEC (2016). 978-1-5090-1919-9.

[56] Novais, Susana; Nascimento, Micael; Grande, Lorenzo; Domingues, Maria Fátima; Antunes, Paulo; Alberto, Nélia; Leitão, Cátia; Oliveira, Ricardo; Koch, Stephan; Kim, Guk Tae; Passerini, Stefano; Pinto, João. Internal and External Temperature Monitoring of a Li-Ion Battery with Fiber Bragg Grating Sensors. Sensors (Basel, Switzerland). 16 (2016).

[57] Lewerenz, Meinert; Münnix, Jens; Schmalstieg, Johannes; Käbitz, Stefan; Knips, Marcus; Sauer, Dirk Uwe. Systematic aging of commercial LiFePO 4 |Graphite cylindrical cells including a theory explaining rise of capacity during aging. Journal of Power Sources. 345 (2017).

[58] Friesen, Alex; Mönnighoff, Xaver; Börner, Markus; Haetge, Jan; Schappacher, Falko M.; Winter, Martin. Influence of temperature on the aging behavior of 18650-type lithium ion cells. Journal of Power Sources. 342 (2017).

[59] Peter Keil, Dipl.-Ing. Univ. Aging of Lithium - Aging of Lithium-Ion Batteries in Electric Vehicles. Technischen Universität München (19.06.2017).

[60] Wu, Yao; Keil, Peter; Schuster, Simon F.; Jossen, Andreas. Impact of Temperature and Discharge Rate on the Aging of a LiCoO2/LiNi0.8Co0.15Al 0.05O2 Lithium-Ion Pouch Cell. Journal of The Electrochemical Society. 164 (2017).

List of Figures

List of Tables